Electrical Power and Energy Systems 104 (2019) 744–771

Contents lists available at ScienceDirect

Electrical Power and Energy Systems

journal homepage: www.elsevier.com/locate/ijepes

Load flow balancing and transient stability analysis in renewable integrated power grids☆

Muhammad Adnan[a], Muhammad Tariq[a,*], Zhenyu Zhou[b], H. Vincent Poor[c]

[a] National University of Computer and Emerging Sciences, Pakistan
[b] State Key Laboratory of Alternate Electrical Power System with Renewable Energy Sources, School of Electrical and Electronic Engineering, North China Electric Power University, Beijing 102206, China
[c] Electrical Engineering Department, Princeton University, NJ, 08544, USA

ARTICLE INFO

Keywords:
Load flow balancing
Transient stability
Single and multiple interval faults
Renewable integrated power grid

ABSTRACT

Due to random patterns of demand response from the consumer side and the unreliable nature of renewable energy resources, load flow balancing and transient stability become challenging issues in power systems. They are even more challenging in cases of multiple interval three phase (L-L-L) faults (MITPFs), which arise in power systems due to power quality disturbances. The intent of this work is to examine the influence of MITPFs on renewable energy resources (RERs) for load flow balancing and transient stability analysis. Wind turbine power dispatchability and uncertainty have a significant impact on load flow balancing and transient stability, especially in cases of occurrence of MITPFs. Probabilistic modeling is performed in this paper to formulate the complexity of randomness for load flow balancing through a smart node and transient stability analysis through a unified power flow controller. The proposed probabilistic algorithm is based on the deviations between generation and demand response patterns due to an MITPF. An autocorrelation expansion is applied to approximate the randomness of probabilistic variables between the forecast generation and actual response pattern. Future contingencies can be predicted before disruptive changes arise due to the occurrence of an MITPF using the above probabilistic analysis. Simulation results show that the proposed algorithm outperforms existing alternatives and can achieve near optimal performance for a wide range of load variations and power quality disturbances in renewable-integrated power grids.

1. Introduction

The economic prosperity of any country relies upon its electric power infrastructure. A stronger electric power infrastructure that incorporates advanced sensing, communication, security and control technologies in the form of a smart grid can provide a more reliable, efficient, sustainable and economical supply of electricity [1,2]. One of the key features of smart grids is to utilize renewable energy resources (RERs) within a renewable integrated power grid (RIPG), in order to meet consumer side load requirements for providing cheaper electricity [1]. However, there are also certain limitations involved with RIPGs, and the most important one is reliability, which must be resolved in order to provide a secure and sustainable form of electric energy to consumers [3]. Incorporating certain flexible AC transmission system (FACTS) devices into the RIPG, such as static compensators (STATCOMs), static synchronous series compensators (SSSCs) and unified power flow controllers (UPFCs), provides a promising way to address reliability issues in power systems. Among these, UPFCs are a versatile form of FACTS devices, which are capable of both shunt and series compensation in order to mitigate the effects of power quality disturbances in a power system [4]. Moreover, there are also various technical issues associated with RIPGs. One such issue is power quality disturbances and their adverse affects, which account for both load flow balancing and transient sta-

☆ This work was supported in part by the U.S. National Science Foundation under Grants DMS-1736417 and ECCS-1824710.
* Corresponding author.
E-mail address: tariq.khan@nu.edu.pk (M. Tariq).

https://doi.org/10.1016/j.ijepes.2018.06.037
Received 13 March 2018; Received in revised form 10 May 2018; Accepted 18 June 2018
Available online 04 August 2018

bility. These power quality disturbances occur in power systems due to the occurrence of different types of faults. An RIPG reacts adversely to power quality issues depending on the severity of the problem, i.e., type of fault. In this paper, an analysis of different line fault types is conducted based on their durations to clearly illustrate the difference between single interval three phase (L-L-L) faults (SITPFs) and multiple interval three phase (L-L-L) faults (MITPFs) and their impact on RIPGs for load flow balancing and transient stability. MITPFs occur in power systems due to, for example, lightning strikes on a transmission line over multiple time periods, resulting in closing and opening of a circuit breaker at multiple times. Such MITPFs have adverse effects on RIPGs in terms of multiple power dispatchability and transient stability issues.

Load flow balancing and transient stability are challenging tasks in cases of single interval faults in RIPGs. They are even more challenging in cases of multiple interval faults, where fault analysis patterns are more random and their adverse effects are more severe. Various strategies have been adopted and techniques have been developed for load flow balancing and transient stability using UPFCs in RIPGs. The techniques for load flow balancing can be divided into several categories. For example, some techniques address the problem of power balancing in a general RIPG with storage and flexible loads [5]. Alternatively, the development of a dynamic optimum power flow framework to model curtailment of renewable distributed generation, energy storage systems and flexible demand for multiple time periods, is discussed in [6]. The improvements made by using electric vehicle (EV) chargers and photo-voltaic (PV) inverters that can balance the network, are further considered in [7]. Another approach for load flow balancing is to control stored energy to balance power generation of renewable sources to optimize overall power consumption at the microgrid (MG) level [8]. Furthermore, several probabilistic approaches have also been proposed, in order to deal with the uncertainty involved with RERs. These include the design of novel probabilistic power flow and probabilistic optimal power flow algorithms to reduce uncertainties due to environmental impacts on PV and wind farm generation [9–11]. Addressing the problem of different charging and discharging behaviors of EVs with the integration of PV generation and wind power generation in terms of probabilistic load flow modeling is also proposed in [12,13].

A common drawback of the above works is that all of these techniques require sophisticated storage, flexible loads and control mechanisms in order to provide effective load flow balancing on the receiving side of power grid stations. Moreover, these proposed approaches are computationally expensive and the optimal solutions in terms of load flow balancing are not guaranteed, considering larger deviations between loads, i.e., from KW to MW. To cover this gap, this work introduces a new solution method to this problem: a smart node transmission network topology that integrates different RERs with one another in order to accommodate load flow balancing in an RIPG, keeping variable heavy loads in mind. To the best of the authors' knowledge, this is the first work that addresses design of a customized smart node in order to stabilize the power system for load flow balancing on the receiving side, even in cases of occurrence of either SITPFs or MITPFs. The smart node is basically an intelligent interconnection of the transmission network that takes into account uncertainties in loads and renewable energy resources due to SITPFs or MITPFs and improvises the load flow balancing on the receiving side, based on the potential vulnerability of an RIPG.

Similarly, in order to address transient stability issues in power systems, various solutions have been proposed in [14–29].

Transient behavior is quantified with the inclusion of UPFCs, incorporating dynamic control strategies for power flow and voltage profile on different buses in [14,15]. A pattern recognition based solution for fault analysis, fault-type identification and fault-zone detection in a transmission line with the inclusion of UPFCs is proposed in [16]. Another approach for transient stability analysis is based on the design of a generic algorithm for simulating system transient stability for any type of fault for three and six phase systems [17].

In recent years, various approaches have been considered for transient stability enhancement in RIPGs using UPFCs. In [18,19], the authors considered UPFCs for simultaneous power flow control, and transient stability enhancement of hybrid power systems, i.e., for large interconnections, and correspondingly addressed the complexity of such power systems. Similarly, analyzing power quality disturbances for transient stabilities due to single line to ground (SLG), double line to ground (DLG) and triple line to ground (TLG) faults, i.e., SITPFs, and their compensation using FACTS devices was discussed in [20]. Also, characterizing UPFC energy functions in terms of Lyapunov energy functions, in order to determine the effect of UPFCs on transient stability enhancement, considering the occurrence of three phase short circuit faults in power systems during a single interval has been investigated in [21]. Addressing an issue of how to control UPFC parameters in order to achieve the maximal desired effect in solving the first swing stability problem in case of occurrence of an SITPF was proposed in [22,23]. Moreover, in order to control the entire flow of load and voltage sags/flickers, while eliminating harmonics simultaneously in cases of occurrence of different grid faults based on single intervals, [24] proposed an inventive systematic approach based on operating the UPFC in an optimal control mode to efficiently manage these power quality disturbances. Similarly, the stability assessment for the occurrence of SITPFs without FACTS controllers in the power network and then with the FACTS controllers was proposed in [25] to clarify the impact of SITPFs on the performance of wind turbines and transient rating of the FACTS controllers for enhancement of transient stability issues. Another approach is to consider multiple modes of oscillations due to the occurrence of a three phase to ground fault during a single interval and its compensation using a UPFC as was proposed in [26]. Similarly, tuning the gains of a UPFC controller with a simple Genetic Algorithm (GA) to address transient stability issues in cases of the occurrence of SITPFs was proposed in [27]. Furthermore, damping of the low frequency oscillations of multi-machine multi-UPFC power systems based on an adaptive input-output feedback linearization control (AIFLC) approach, considering an SITPF, was proposed in [28]. The same scenario of damping low frequency oscillations using a particle swarm optimization based output feedback UPFC damping controller, considering a 6 cycle SITPF, was investigated in [29]. All of these techniques were applied to RIPGs for compensating power quality disturbances using FACTS devices, by incorporating small delays that occurred due to SITPFs. However, the

utilization of UPFCs for transient stability enhancement in cases of occurrence of MITPFs has not been discussed in the literature. In the case of an MITPF, each time a power system is restored to its original condition, the disturbance level (i.e., the transient level) increases, due to corresponding larger fault delays in the power system. Due to these adverse power quality issues, the system's restoring capability becomes weak, which makes it potentially more vulnerable to occurrences of MITPFs. Moreover, if faults persist for a certain interval of time in this situation, then the power system will become unstable. Therefore, mitigation for power system stability in that case is difficult to achieve.

In this paper, we analyze the effects of power quality disturbances that occur in an RIPG due to transient stability issues, which arise in cases of occurrence of SITPFs or MITPFs. Transient stability is a term that is reserved in the power systems literature for angle stability under large disturbances, whereas, power quality disturbances is a term that is related to transients, interruptions, voltage sags and swells, waveform distortion, voltage fluctuations and frequency variations; however there is a strong cause and effect relationship between these two types of phenomena [30]. Transient stability can be defined as the stability of a power system to maintain synchronization when subjected to a large disturbance, i.e., in our case, occurrence of an MITPF in the RIPG. These severe disturbances result in large excursions of wind turbine generator rotor angles, which lead to significant variations in the speed and position of the rotor. Due to these variations, severe power quality issues arise on the receiving side of the RIPG station.

Now, in order to address these transient stability issues, which lead to power quality disturbances, there are two different possible solutions. The first is to use FACTS devices, i.e., UPFCs, on the generation side to establish a linear power angle relationship among wind turbine generators. This will reduce the variations that arise in the speed and position of the rotors due to the occurrence of SITPFs or MITPFs and correspondingly minimize the power quality issues on the receiving side of the RIPG station. The second approach to address these transient stability issues for minimizing power quality disturbances is to install a UPFC on the receiving side of the RIPG station near the fault occurrence location in order to stabilize the system, even in cases of occurrence of SITPFs or MITPFs. Here we use the second approach. Transient stability oscillations due to the occurrence of faults are of major concern for power system stability, and indeed shall be treated as such. However, in this study these oscillations are discussed from the power quality point of view. In particular, it is claimed that such oscillations can lead to power quality issues. These transient stability issues are characterized in this study using both theoretical and numerical analyses, which lead to the definition of several power quality phenomena that can be induced by such transient stability oscillations as proposed in [30]. The obtained results show that transient stability issues due to the occurrence of SITPFs or MITPFs in an RIPG can indeed be a significant source of power quality problems, as opposed to the widespread empirical belief that these two problems (power system stability and power quality) are not linked to each other [30]. Moreover, the transient stability of a power system with wind turbines also depends on factors such as fault conditions. For example, in the case of an occurrence of an SITPF, less variation arises in the speed and position of the wind turbine rotor, which leads to lesser power quality issues on the receiving side of the RIPG, whereas, considering MITPF, a significant variation in wind turbine rotor speed will causes more substantial power quality issues on the receiving side of RIPG stations.

Load flow balancing and transient stability are growing challenges for SITPFs in power systems and thus can be even more problematic in case of MITPFs. Considering SITPFs, a similar methodology for load flow balancing and transient stability analysis in super smart grids using vehicle to grid (V2G) devices was proposed in [31]. To the best of the authors' knowledge, this is the first work that addresses the analysis based on probabilistic modeling in order to formulate the complexity of randomness for load flow balancing through a smart node and transient stability analysis through a UPFC in an RIPG, in both cases of SITPFs and MITPFs. The proposed probabilistic algorithm is based on the deviations between the generation and demand pattern in case of occurrence of either an SITPF or MITPF. Different parameters can be adjusted, such as demand and supply at a given time, returning demand and nominal reserves, through probabilistic modeling of the smart node. Moreover, considering the complexity of a power system in transient stability analysis, a probabilistic model for the UPFC is proposed based on a scenario of occurrence of an MITPF in the power system.

The key contributions of this paper are as follows:

1. design of a customized smart node transmission network, so that a disturbance at any instance of time in the form of an SITPF or MITPF is compensated as load flow balancing on the receiving side;
2. incorporation of a UPFC into a smart node transmission network in the case of an MITPF, in order to reduce power dispatchability and mitigate transients issues; and
3. development of a probabilistic model to formulate the complexity of randomness for load flow balancing through a smart node and transient stability analysis through a UPFC in an RIPG.The rest of the paper is organized as follow. Section 2 describes the methodology in greater detail. Section 3 compares the proposed methodology with existing load flow balancing and transient stability analysis models via simulation results. Section 4 concludes the paper.

2. Methodology

The proposed methodology consists of two parts. Firstly, the degree of vulnerability of a power system is determined in case of the occurrence of an SITPF or MITPF. To study power system vulnerability, an uncertainty analysis method based on three phase (L-L-L) fault delays is proposed to differentiate the occurrence of an SITPF or MITPF. Moreover, the randomness of load flow due to tripping of certain RERs and power quality issues due to SITPFs or MITPFs are also considered. If a power system is potentially vulnerable to an SITPF or MITPF, then Algorithm 1 below uses the smart node scenario in order to analyze and predict the forecast randomness in a power system by using probabilistic modeling. In other words, remedial action in the form of load flow balancing is performed on the receiving side.

Algorithm 1: Differentiation between SITPFs or MITPFs in a power system.

Input : A set of normal operating states of power system $(n_{a_1}, n_{a_2}, ..., n_{a_n})$
Input : An unexpected outage due to occurrence of three phase (L-L-L) faults at single or multiple intervals $(f_{a_1}, f_{a_2}, ..., f_{a_k})$
//f_{a_1} corresponds to a single interval fault while $f_{a_1} \rightarrow f_{a_k}$ correspond to multiple intervals faults
Input : A set of delays due to occurrence of three phase (L-L-L) faults at single or multiple intervals $(d_{e_1}, d_{e_2}, ..., d_{e_m})$
//d_{e_1} corresponds to a single interval delay while $d_{e_1} \rightarrow d_{e_m}$ correspond to multiple intervals delays
Output: A set of next transition states taken due to occurrence of single or multiple intervals three phase (L-L-L) faults $(t_{r_1}, t_{r_2}, ..., t_{r_j})$
while $(f_{a_1} || f_{a_1} \rightarrow f_{a_k})$ **do**
  assign the next transition state to compensate for delay d_{e_m} due to occurrence of single or multiple intervals three phase (L-L-L) faults
  //SITPF f_{a_1} or MITPF $f_{a_1} \rightarrow f_{a_k}$ occurred, which causes a delay d_{e_m} in the power system
  if $(delay = d_{e_m} + d_{e_{m+1}})$ **then**
    Next transition, $t_{r_{j+1}} \rightarrow Smartnode/SITPF$
  //Delay with an estimated threshold, i.e., 1s for an SITPF
  else if $(delay = d_{e_m} + d_{e_{m+5}})$ **then**
    Next transition, $t_{r_j+1} \rightarrow Smartnode/MITPF$
  //Delay above an estimated threshold of 1s, i.e., 5s for an MITPF
  else if $(delay = (d_{e_m} + d_{e_{m+6}}) \rightarrow (d_{e_m} + d_{e_{m+8}}) \rightarrow (d_{e_m} + d_{e_{m+10}}))$ **then**
    The next transition, $t_{r_{j+1}} \rightarrow Upfc/MITPF$
  //To compensate multiple power dispatchability delays
  else if $(delay = (d_{e_m} + d_{e_{m+2}}) \rightarrow (d_{e_m} + d_{e_{m+2.5}}) \rightarrow (d_{e_m} + d_{e_{m+3}}))$ **then**
    The next transition, $t_{r_{j+1}} \rightarrow Upfc/MITPF$
  //To compensate multiple transients delays
  else
    The next transition, $t_{r_{j+1}} \rightarrow (n_{a_1} \rightarrow n_{a_n})$
  //The power system is operating in its normal state
  end
  Send $t_{r_{j+1}}$ transition state as an input to Algorithm 1
end

Secondly, Algorithm 1 is used to facilitate transient stability analysis and power outages in a power system using probabilistic modeling, so that in case of an MITPF, a decision in terms of switching of the UPFC on the receiving side is performed. Smart nodes are operated at the receiving end in case of either an SITPF or an MITPF with corresponding smaller or larger delays, in terms of variations in the d_{e_m} parameter, i.e., above an estimated threshold, 1s, which decides the potential vulnerability to an occurrence of an SITPF or MITPF. For an SITPF, the delay is $(delay = d_{e_m} + d_{e_{m+1}})$ and for an MITPF, the delay is $(delay = d_{e_m} + d_{e_{m+5}})$. Where, d_{e_m} represents delay at a given time and $d_{e_{m+k}}$ represents the fault delay of either an SITPF or MITPF. Similarly, the UPFC is operated on the receiving side; if the delay parameter d_{em} is above the estimated threshold range, i.e., 1s for an SITPF, it triggers the next transition state $t_{r_{j+1}}$ for operating the UPFC in the RIPG in case of an MITPF. We consider the use of a UPFC only for the case of an MITPF in order to reduce multiple power dispatchabilty delays, i.e., $(delay = (d_{e_m} + d_{e_{m+6}}) \rightarrow (d_{e_m} + d_{e_{m+8}}) \rightarrow (d_{e_m} + d_{e_{m+10}}))$ and multiple transients delay issues, i.e., $(delay = (d_{e_m} + d_{e_{m+2}}) \rightarrow (d_{e_m} + d_{e_{m+2.5}}) \rightarrow (d_{e_m} + d_{e_{m+3}}))$, as using UPFCs for SITPFs has already been treated in the literature. Also, we are dealing with transient issues, which arise in the RIPG in cases of occurrence of SITPFs or MITPFs and if proper remedial action is not taken, then these transient issues lead to significant damage in the form of equipment failures as noted in [32,33]. These transient issues are potentially destructive and can cause electronic systems to fail. Moreover, as previously discussed, a comparative analysis in terms of arising power quality disturbances, i.e., transients, due to SITPFs or MITPFs and their severe impact on the RIPG leads to a conclusion that occurrence of an MITPF in a power system leads to significant transient issues in the RIPG, which need to be properly addressed through using the UPFC. Moreover, due to lower wind power dispatchability, i.e., supply from the wind turbines towards receiving side connected loads is not constant, especially in case of occurrence of faults, incorporation of UPFCs is necessary, especially in case of occurrence of an MITPF. These case

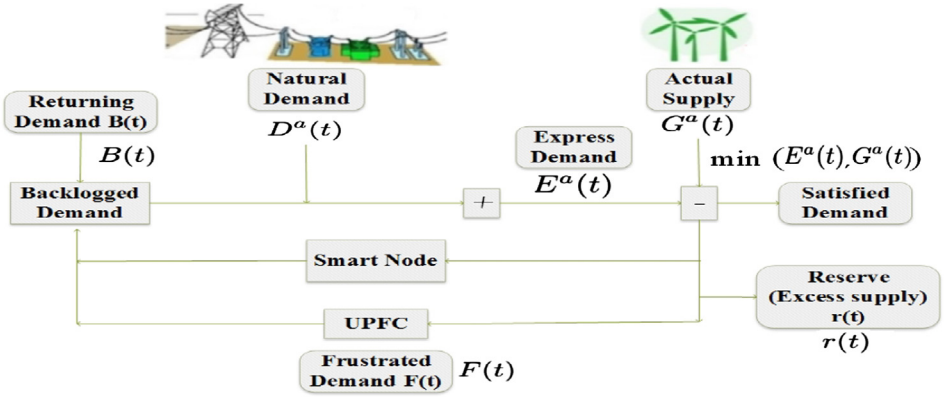

Fig. 1. Demand response schematic model.

scenarios are also verified by simulation results in Section 3.

Fig. 1 shows the demand response schematic as a closed loop control system for probabilistic modeling of load flow balancing and transient stability in the RIPG. The closed loop in the form of a smart node and UPFC will continuously monitor the power system, and proper remedial action will be taken for load flow balancing and transient stability. The smart node properly optimizes the power system for load flow balancing in case of an SITPF, while for an MITPF, incorporating a UPFC in the smart node transmission network is necessary to completely optimize the power system for load flow balancing, in terms of reducing multiple power dispatchability and transients. Details regarding the terms used in Fig. 1 are discussed in the next section.

2.1. Smart node probabilistic modeling for a single interval three phase (L-L-L) fault

The reliability of a power grid is directly affected by the integration of large scale RERs, and this effect can be even more severe in the presence of disturbances. We investigate the issue of power flow balancing in a synchronized network of three RERs, with the occurrence of either an SITPF or MITPF, by using the concept of a smart node. A closed loop control system model of a transmission grid is formed with large penetrations of:

1. demand response, and
2. power quality disturbances.

The demand response penetrations occur due to tripping of RERs with the occurrence of SITPFs or MITPFs. Power quality issues are more prominent in case of an MITPF as compared to an SITPF, due to multiple transients and power dispatchability. In order to analyze the future contingencies in a power system due to an SITPF or MITPF, we consider a scenario of forecast demand $D^f(t)$ and forecast supply $G^f(t)$. Moreover, in order to meet synchronization between the generation and demand, the $G^f(t)$ must be synchronized with $D^f(t)$, i.e.,

$$G^f(t) = D^f(t) + r_o, \tag{1}$$

where, r_o is a nominal reserve, i.e., supply from the smart node, in order to accommodate load flow balancing between $G^f(t)$ and $D^f(t)$. In this scenario, we capture the effect of the response by modifying the returning demand $B(t)$, in terms of adjusting r_o through the smart node, in order to achieve synchronization between $G^f(t)$ and $D^f(t)$.

Suppose that an RIPG is potentially vulnerable to an SITPF. Assume $1/\lambda$ to be a delay time slot. The average delay A due to occurrence of an SITPF can be calculated as

$$A = \frac{1}{\lambda}. \tag{2}$$

The above average delay corresponds to one time slot due to occurrence of an SITPF. A more generalized form of (2), in terms of a closed loop probabilistic model is

$$A = \frac{1}{\sum_{i_1=1}^{n_1} \lambda_{i_1}}, \tag{3}$$

where λ_{i_1} represents the SITPF delay parameter for each iteration, in terms of the closed loop probabilistic model and n_1 represents the effect of the SITPF on a synchronized network of three RERs, i.e., $(n_1 = 3)$.

Similarly, in order to address the real time scenario of demand response, we consider the actual demand $D^a(t)$ to be synchronized with $D^f(t)$, along with some randomness $R_D(t)$, i.e.,

$$D^a(t) = D^f(t) + R_D(t). \tag{4}$$

By incorporating the average delay in (3) due to occurrence of an SITPF into (4), it can be rewritten as,

$$D^a(t) = \left\{ \left[D^f(t) \times \left(\frac{1}{\sum_{i_1=1}^{n_1} \lambda_{i_1}} \right) \right] + R_D(t) \right\}. \tag{5}$$

To continuously monitor the power system, in terms of closed loop control, (5) can be rewritten in the form of generalized expression as

$$D^a(t) = \sum_{i=1}^{n} \left\{ \left[D_i^f(t) \times \left(\frac{1}{\sum_{i_1=1}^{n_1} \lambda_{i_1}} \right) \right] + R_{D_i}(t) \right\}, \tag{6}$$

where $R_D(t)$ is the deviation between $D^a(t)$ and $D^f(t)$, which can be determined by the autocorrelation, i.e.,

$$R_D(t) = E[D^a(t) D^f(t)]. \tag{7}$$

When, $D^a(t) \to D^f(t)$, the random deviation $R_D(t) \to 0$, which makes the system stable as

$$G^f(t) = D^f(t). \tag{8}$$

Similarly, in order to address the real time scenario of generation response, we consider the actual supply $G^a(t)$ to be equal to the previous supply $G(t-1)$ and $G^f(t)$ along with some randomness $R_G(t)$,

$$G^a(t) = G(t-1) + G^f(t) + R_G(t), \tag{9}$$

where, $G(t-1)$ is the control parameter, which returns a closed loop to the previous time slot in real time, in order to adjust the demand pattern with the generation response.

Now, by incorporating the average delay in (3) into (9) and in terms of the closed loop probabilistic model, (9) can be rewritten in a generalized form as,

$$G^a(t) = \sum_{i=1}^{n} \left\{ \left[G_i(t-1) \times \left(\frac{1}{\sum_{i_1=1}^{n_1} \lambda_{i_1}} \right) \right] + \left[G_i^f(t) \times \left(\frac{1}{\sum_{i_1=1}^{n_1} \lambda_{i_1}} \right) \right] + R_{G_i}(t) \right\}, \tag{10}$$

where $R_G(t)$ shows the deviation between $G^a(t)$ and $G^f(t)$, and it can also be determined using an autocorrelation, i.e.,

$$R_G(t) = E[G^a(t)G^f(t)]. \tag{11}$$

Similarly, when, $G^a(t) \to G^f(t)$, the random deviation $R_G(t) \to 0$, which stabilizes the power system in terms of synchronous stability between $G^f(t)$ and $D^f(t)$.

Moreover, in order to make $R_G(t) \to 0$, $G(t-1)$, i.e., the control parameter, should be properly adjusted to achieve synchronous stability between $G^f(t)$ and $D^f(t)$.

Moreover, the shortage of power due to the SITPF can be represented in terms of the frustrated demand $F(t)$ as,

$$F(t) = E^a(t) - G^a(t), \tag{12}$$

where $E^a(t)$ represents the expressed demand, which should be met at a given time in order to achieve synchronization between generation and demand patterns.

$F(t)$ occurs when

$$E^a(t) > G^a(t). \tag{13}$$

Considering the average delay in (3) due to the SITPF, (12) can be rewritten as

$$F(t) = \left[(E_i^a(t) - G_i^a(t)) \times \left(\frac{1}{\sum_{i_1=1}^{n_1} \lambda_{i_1}} \right) \right]. \tag{14}$$

Using the generalized expression in terms of the closed loop probabilistic model, (14) can be rewritten as

$$F(t) = \sum_{i=1}^{n} \left[\left(\frac{E_i^a(t) - G_i^a(t)}{n} \right) \times \left(\frac{1}{\sum_{i_1=1}^{n_1} \lambda_{i_1}} \right) \right]. \tag{15}$$

$F(t)$ will fed back to the power system as a backlogged demand $B(t)$, i.e., returning demand, but with the addition of some loop delay parameter, i.e., λ_{c_1}. Therefore, the backlogged demand $B(t)$ will be equal to $F(t)$ times the closed loop corresponding delay parameter λ_{c_1},

$$B(t) = \left(\frac{1}{\sum_{c_1=1}^{n_1} \lambda_{c_1}} \right) \times (E^a(t) - G^a(t)). \tag{16}$$

Incorporating the delay due to the SITPF in (3) and expressing $B(t)$ in terms of the generalized form, (16) can be rewritten as

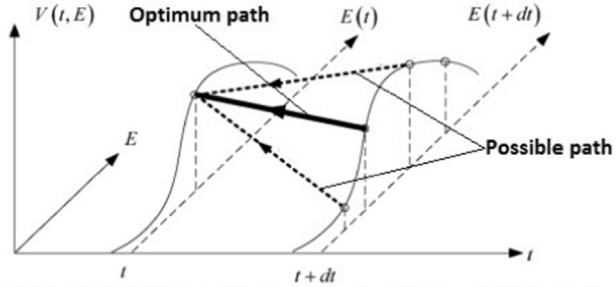

Fig. 2. Backward recursion process for a single storage [8] device.

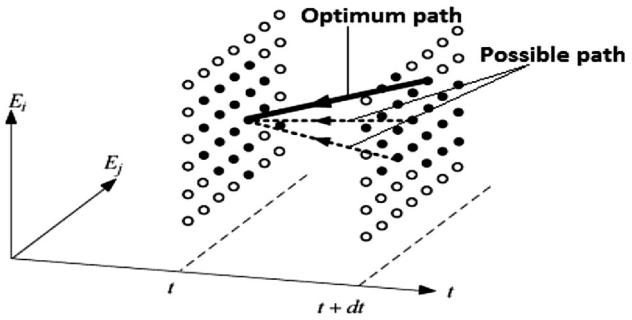

Fig. 3. Backward recursion process for two storage devices [8].

$$B(t) = \left(\frac{1}{\sum_{c_1=1}^{n_1} \lambda_{c_1}} \right) \times \sum_{i=1}^{n} \left[\left(\frac{E_i^a(t) - G_i^a(t)}{n} \right) \times \left(\frac{1}{\sum_{i_1=1}^{n_1} \lambda_{i_1}} \right) \right]. \tag{17}$$

Similarly, the reserve $r(t)$ can be expressed as

$$r(t) = G^a(t) - E^a(t). \tag{18}$$

The power system should be in a reserve state when

$$G^a(t) > E^a(t), \tag{19}$$

while, considering the average delay in (3) and the generalized expression in terms of the closed loop probabilistic model, (18) can be rewritten as

$$r(t) = \sum_{i=1}^{n} \left[(G_i^a(t) - E_i^a(t)) \times \left(\frac{1}{\sum_{i_1=1}^{n_1} \lambda_{i_1}} \right) \right]. \tag{20}$$

The threshold policy for reserve $r(t)$ should be: if,

$$r(t) < r_o, \tag{21}$$

then increase $G^a(t)$ through the smart node, in order to make $r(t)$ come as close to r_o as possible (considering the ramp up constraints); otherwise, if,

$$r(t) > r_o, \tag{22}$$

then, decrease $G^a(t)$ in order to make $r(t)$ come as close to r_o as possible (considering the ramp down constraints). Here, the ramping constraint are,

$$r_o \leqslant G(t) - G(t-1) \leqslant r_o. \tag{23}$$

From (9), $G(t) - G(t-1)$ can be represented as

$$r_o \leqslant G^f(t) + R_G(t) \leqslant r_o. \tag{24}$$

The problem is to keep the returning or backlogged demand, i.e., $B(t)$, stable by minimizing $R_G(t)$ through the smart node. This can be achieved by controlling $r(t)$ to be synchronized with r_o, considering ramping up and ramping down constraints from (21) and (22). Minimizing $R_G(t)$, (24) can be represented as

$$r_o \leqslant G^f(t) \leqslant r_o. \tag{25}$$

From (1), $G^f(t)$ can be synchronized to $D^f(t)$, i.e., (25) can be represented as

$$r_o \leqslant D^f(t) \leqslant r_o. \tag{26}$$

Through (26), synchronous stability between the demand and generation response pattern can be achieved in case of occurrence of an SITPF. In the following subsection we perform similar modeling for the case of an MITPF.

2.2. Smart node probabilistic modeling for a multiple interval three phase (L-L-L) fault

Suppose that an RIPG is potentially vulnerable to an MITPF. Then,

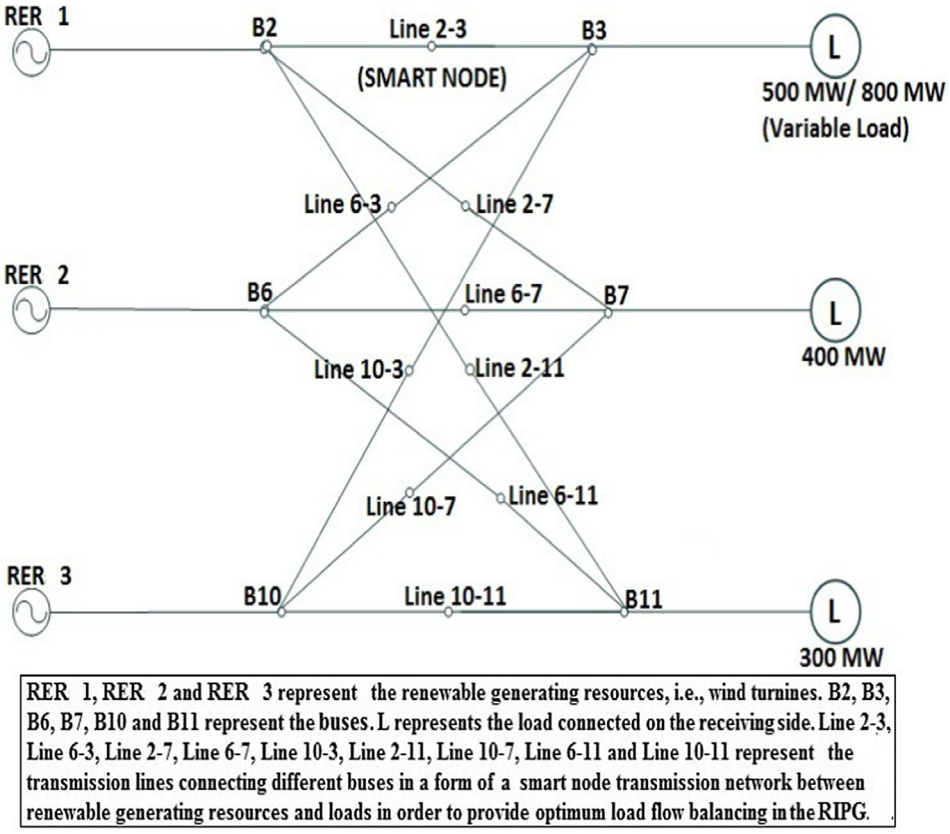

Fig. 4. Smart node scale free graph topological model.

the average delay A in (3) will now become

$$A = \frac{1}{\sum_{i_1=1}^{n_1} \lambda_{i_1} + \sum_{i_2=1}^{n_2} \lambda_{i_2} + \sum_{i_3=1}^{n_3} \lambda_{i_3}}, \tag{27}$$

where $n_1 = 3$, $n_2 = 3$, and $n_3 = 3$, i.e., we assume three RERs. In this case, the effect of the MITPF is simultaneous, i.e., it depends on multiple intervals of time. Moreover, λ_{i_1}, λ_{i_2} and λ_{i_3} correspond to the first, second and third interval three phase fault delay parameter of the three RERs. Considering (27) in terms of the multiple fault delays parameter $\lambda_{i_{mfd}}$, i.e.,

$$\sum_{i_{mfd}}^{n_{mfd}} \lambda_{i_{mfd}} = \sum_{i_1=1}^{n_1} \lambda_{i_1} + \sum_{i_2=1}^{n_2} \lambda_{i_2} + \sum_{i_3=1}^{n_3} \lambda_{i_3}, \tag{28}$$

where, $n_{mfd} = n_1 + n_2 + n_3$ and $i_{mfd} = i_1 + i_2 + i_3$, then, (27) will become

$$A = \frac{1}{\sum_{i_{mfd}}^{n_{mfd}} \lambda_{i_{mfd}}}. \tag{29}$$

$D^a(t)$ and $G^a(t)$ in (6) and (10) will become

$$D^a(t) = \sum_{i=1}^{n} \left\{ \left[D_i^f(t) \times \left(\frac{1}{\sum_{i_{mfd}}^{n_{mfd}} \lambda_{i_{mfd}}} \right) \right] + R_{D_i}(t) \right\}, \tag{30}$$

$$G^a(t) = \sum_{i=1}^{n} \left\{ \left[G_i(t-1) \times \left(\frac{1}{\sum_{i_{mfd}}^{n_{mfd}} \lambda_{i_{mfd}}} \right) \right] + \left[G_i^f(t) \times \left(\frac{1}{\sum_{i_{mfd}}^{n_{mfd}} \lambda_{i_{mfd}}} \right) \right] + R_{G_i}(t) \right\}. \tag{31}$$

Similarly, $F(t)$, $B(t)$, and $r(t)$ in (14), (17), and (20) will become

$$F(t) = \sum_{i=1}^{n} \left[\left(\frac{E_i^a(t) - G_i^a(t)}{n} \right) \times \left(\frac{1}{\sum_{i_{mfd}}^{n_{mfd}} \lambda_{i_{mfd}}} \right) \right], \tag{32}$$

$$B(t) = \left(\frac{1}{\sum_{c_1=1}^{n_1} \lambda_{c_1}} \right) \times \sum_{i=1}^{n} \left[\left(\frac{E_i^a(t) - G_i^a(t)}{n} \right) \times \left(\frac{1}{\sum_{i_{mfd}}^{n_{mfd}} \lambda_{i_{mfd}}} \right) \right], \tag{33}$$

$$r(t) = \sum_{i=1}^{n} \left[(G_i^a(t) - E_i^a(t)) \times \left(\frac{1}{\sum_{i_{mfd}}^{n_{mfd}} \lambda_{i_{mfd}}} \right) \right]. \tag{34}$$

2.3. Transient stability analysis for a multiple interval three phase (L-L-L) fault

UPFCs are the most versatile form of FACTS devices for enhancing the stability of power systems. A UPFC can compensate a power system, both in terms of series as well as shunt configurations. The impact of UPFC control modes on power system reliability has not been addressed sufficiently in the literature, especially in the case of MITPFs. Considering the above scenario, suppose that an RIPG is potentially vulnerable to MITPFs. The average delay A in terms of an MITPF in (27) will now become

$$A = \left[\left(\frac{1}{\sum_{i_1=1}^{n_1} \lambda_{i_1} + \sum_{i_2=1}^{n_2} \lambda_{i_2} + \sum_{i_3=1}^{n_3} \lambda_{i_3}} \right) + \left(\frac{1}{\sum_{i_4=1}^{n_4} \lambda_{i_4} + \sum_{i_5=1}^{n_5} \lambda_{i_5} + \sum_{i_6=1}^{n_6} \lambda_{i_6}} \right) \right], \tag{35}$$

where, λ_{i_1}, λ_{i_2} and λ_{i_3} represent the delays parameter incurred in terms of transients and λ_{i_4}, λ_{i_5} and λ_{i_6} represent the delays parameter incurred in terms of power dips in a synchronized network of three RERs, due to an MITPF. Here, $n_1 = 3$, $n_2 = 3$ and $n_3 = 3$ and $n_4 = 3$, $n_5 = 3$ and $n_6 = 3$, i.e., transient and power dip effects due to the MITPF span up to three intervals. Considering (35) in terms of transient ($\lambda_{i_{trd}}$) and

power dip ($\lambda_{i_{pdd}}$) delays parameter, we have

$$\sum_{i_{trd}}^{n_{trd}} \lambda_{i_{trd}} + \sum_{i_{pdd}}^{n_{pdd}} \lambda_{i_{pdd}} = \left[\left(\sum_{i_1=1}^{n_1} \lambda_{i_1} + \sum_{i_2=1}^{n_2} \lambda_{i_2} + \sum_{i_3=1}^{n_3} \lambda_{i_3}\right) + \left(\sum_{i_4=1}^{n_4} \lambda_{i_4} + \sum_{i_5=1}^{n_5} \lambda_{i_5} + \sum_{i_6=1}^{n_6} \lambda_{i_6}\right)\right], \tag{36}$$

where, $n_{trd} = n_1 + n_2 + n_3$, $i_{trd} = i_1 + i_2 + i_3$, $n_{pdd} = n_4 + n_5 + n_6$ and $i_{pdd} = i_4 + i_5 + i_6$. Eq. (35) will become

$$A = \left[\frac{1}{\sum_{i_{trd}}^{n_{trd}} \lambda_{i_{trd}}} + \frac{1}{\sum_{i_{pdd}}^{n_{pdd}} \lambda_{i_{pdd}}}\right]. \tag{37}$$

$D^a(t)$ and $G^a(t)$ in (30) and (31) will become

$$D^a(t) = \sum_{i=1}^{n} \left\{\left[D_i^f(t) \times \left(\frac{1}{\sum_{i_{trd}}^{n_{trd}} \lambda_{i_{trd}}} + \frac{1}{\sum_{i_{pdd}}^{n_{pdd}} \lambda_{i_{pdd}}}\right)\right] + R_{D_i}(t)\right\}, \tag{38}$$

$$G^a(t) = \sum_{i=1}^{n} \left\{\left[G_i(t-1) \times \left(\frac{1}{\sum_{i_{trd}}^{n_{trd}} \lambda_{i_{trd}}} + \frac{1}{\sum_{i_{pdd}}^{n_{pdd}} \lambda_{i_{pdd}}}\right)\right] + \left[G_i^f(t) \times \left(\frac{1}{\sum_{i_{trd}}^{n_{trd}} \lambda_{i_{trd}}} + \frac{1}{\sum_{i_{pdd}}^{n_{pdd}} \lambda_{i_{pdd}}}\right)\right] + R_{G_i}(t)\right\}. \tag{39}$$

Similarly, $F(t)$, $B(t)$, and $r(t)$ in (32), (33) and (34) will become

$$F(t) = \sum_{i=1}^{n} \left[\left(\frac{E_i^a(t) - G_i^a(t)}{n}\right) \times \left(\frac{1}{\sum_{i_{trd}}^{n_{trd}} \lambda_{i_{trd}}} + \frac{1}{\sum_{i_{pdd}}^{n_{pdd}} \lambda_{i_{pdd}}}\right)\right], \tag{40}$$

$$B(t) = \left(\frac{1}{\sum_{c_1=1}^{n_1} \lambda_{c_1}}\right) \times \sum_{i=1}^{n} \left[\left(\frac{E_i^a(t) - G_i^a(t)}{n}\right) \times \left(\frac{1}{\sum_{i_{trd}}^{n_{trd}} \lambda_{i_{trd}}} + \frac{1}{\sum_{i_{pdd}}^{n_{pdd}} \lambda_{i_{pdd}}}\right)\right], \tag{41}$$

$$r(t) = \sum_{i=1}^{n} \left[(G_i^a(t) - E_i^a(t)) \times \left(\frac{1}{\sum_{i_{trd}}^{n_{trd}} \lambda_{i_{trd}}} + \frac{1}{\sum_{i_{pdd}}^{n_{pdd}} \lambda_{i_{pdd}}}\right)\right]. \tag{42}$$

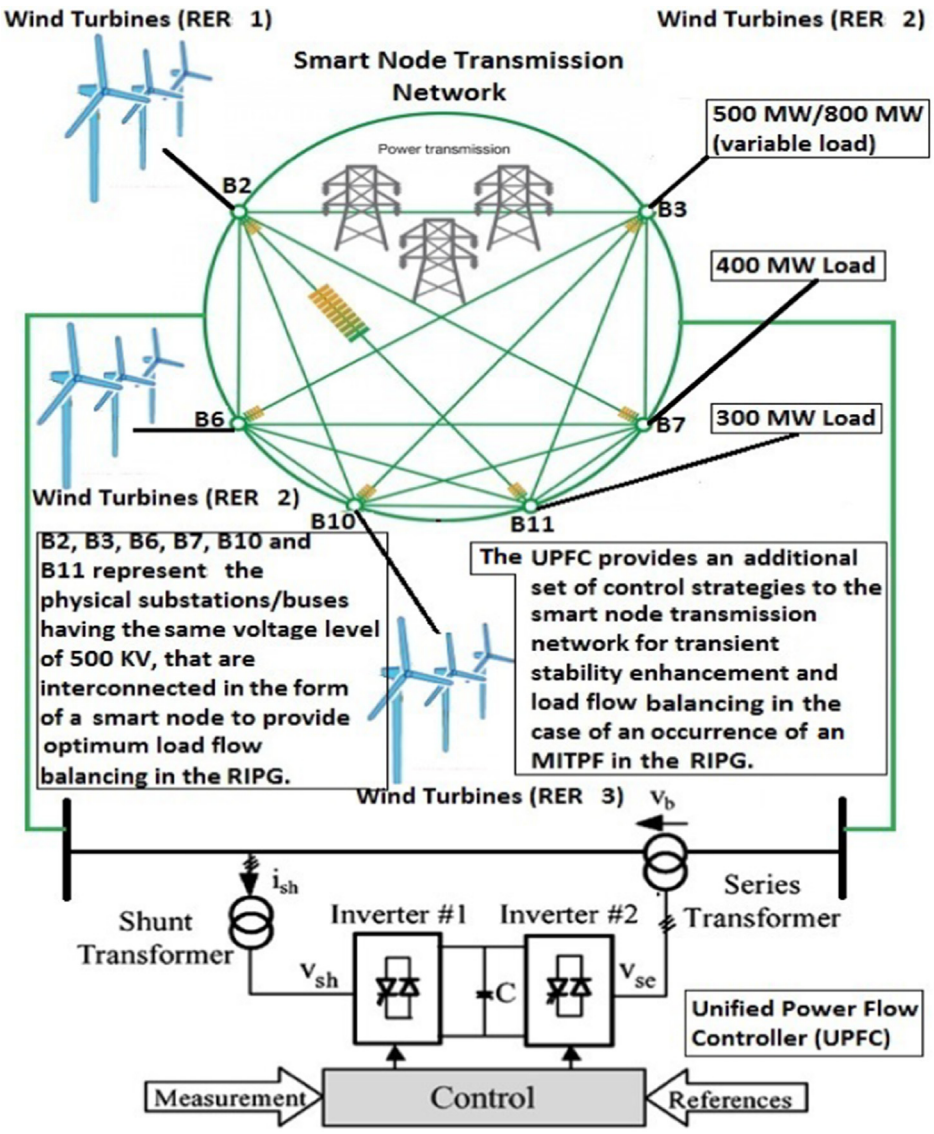

Fig. 5. Smart Node Transmission Network.

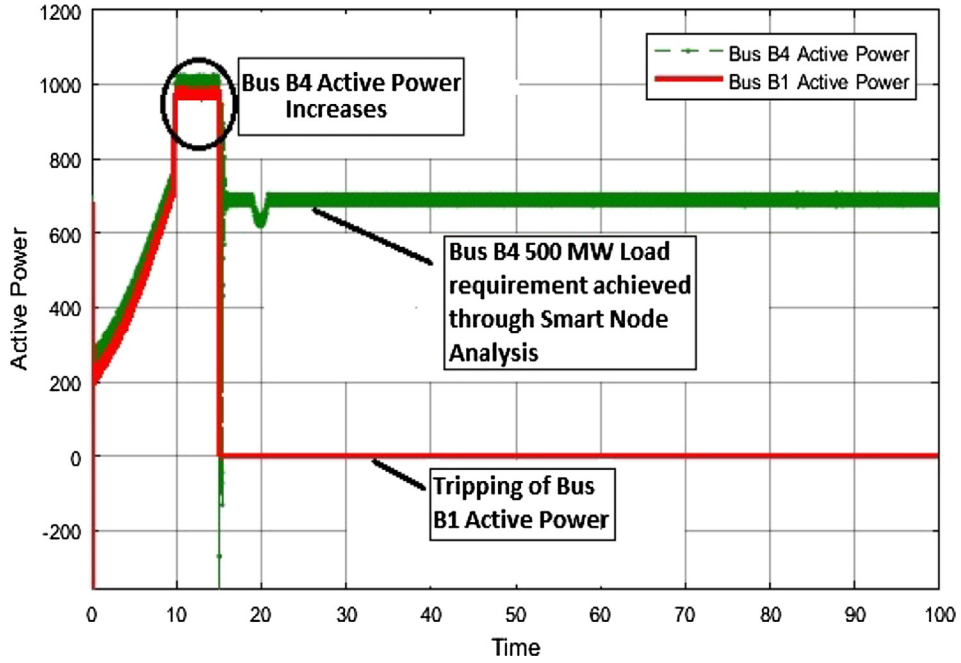

Fig. 6. Buses B1 and B4 active power graphs (SITPF).

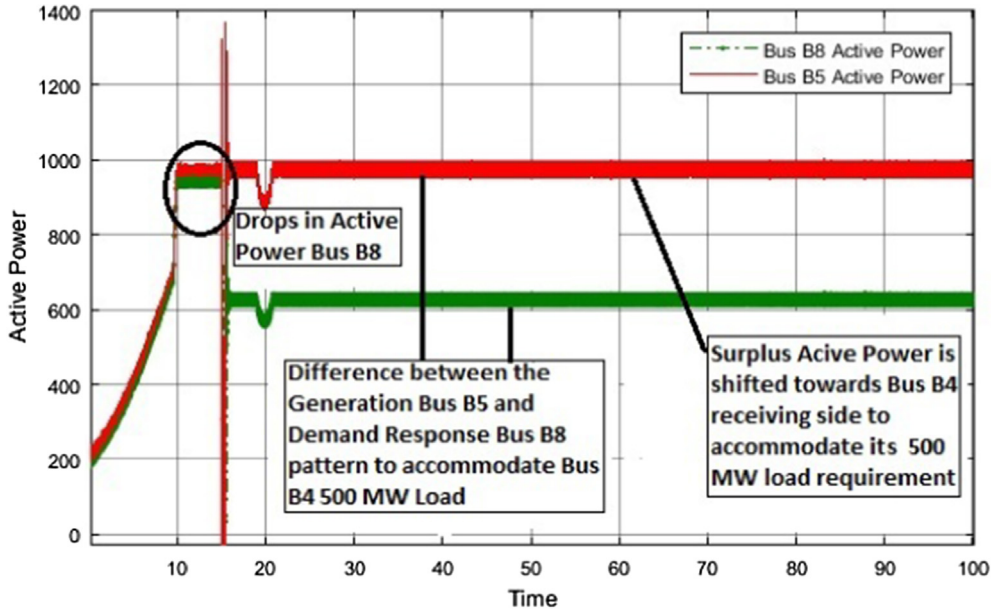

Fig. 7. Buses B5 and B8 active power graphs (SITPF).

The UPFC acts as a power buffer to cope with the volatility of the RERs, i.e., enhancing the power dispatchability and transient stability of the RERs in case of an MITPF. Let us consider a scenario of forecast demands in the case of transients given by $D_{t_1}^f$, $D_{t_2}^f$ and $D_{t_3}^f$ and the forecast RERs to cope with these forecast demands due to the MITPF are $W_{t_1}^f$, $W_{t_2}^f$ and $W_{t_3}^f$. Similarly, consider forecast demands in the case of power dips to be $D_{t_4}^f$, $D_{t_5}^f$ and $D_{t_6}^f$ and the forecast RERs to cope up with these should be $W_{t_4}^f$, $W_{t_5}^f$ and $W_{t_6}^f$. Now, due to the lower power dispatchability of RERs, it is very difficult to cope with transients and power dips with RERs. Therefore, in order to enhance the power dispatchability and transient stability of RERs, we utilize the UPFC. The problem is to compute a dispatched power schedule $P_t^f(t+f)$ in order to increase transient stability and minimize power dispatchability of RERs using the UPFC. This can be done by setting $P_t^f(t+f)$ to $(D_t^f(t+f) - W_t^f(t+f) + r_o)$, where r_o is fixed (positive or negative), using the ramp up and ramp down constraints of (21) and (22). Therefore, the final expression will be

$$\begin{aligned} P_{t_1}^f(t_1+f) + P_{t_2}^f(t_2+f) + P_{t_3}^f(t_3+f) P_{t_4}^f(t_4+f) + P_{t_5}^f(t_5+f) \\ + P_{t_6}^f(t_6+f) = [(D_{t_1}^f(t_1+f) + D_{t_2}^f(t_2+f) + D_{t_3}^f(t_3+f) \\ + D_{t_4}^f(t_4+f) + D_{t_5}^f(t_5+f) + D_{t_6}^f(t_6+f)) \\ -(W_{t_1}^f(t_1+f) + W_{t_2}^f(t_2+f) + W_{t_3}^f(t_3+f) \\ + W_{t_4}^f(t_4+f) + W_{t_5}^f(t_5+f) + W_{t_6}^f(t_6+f)) + r_o]. \end{aligned} \tag{43}$$

3. Simulation results

In order to verify and evaluate the analysis, a series of simulations

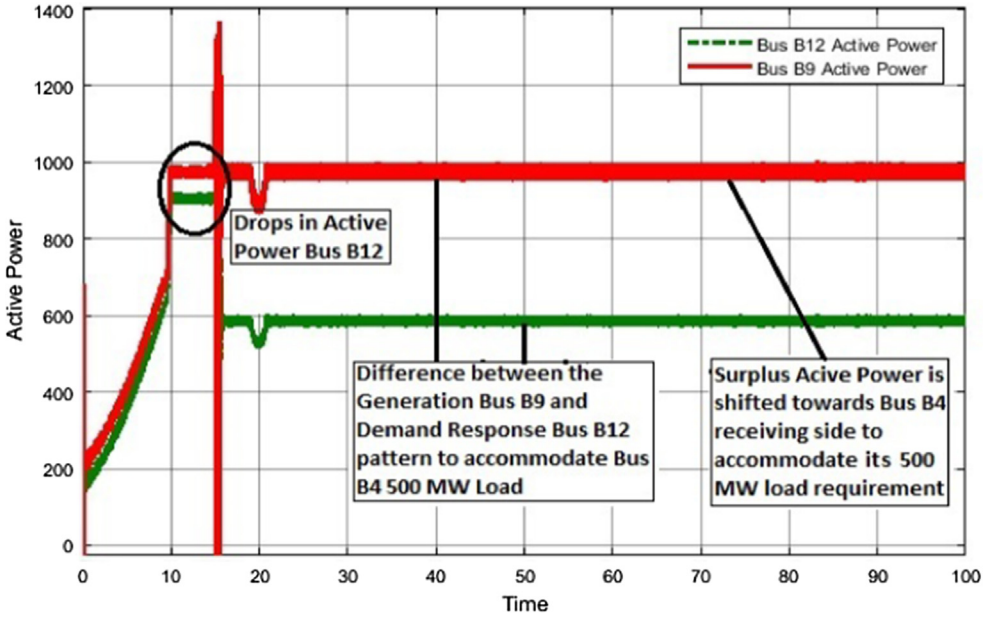

Fig. 8. Buses B9 and B12 active power graphs (SITPF).

Table 1
Active power on different buses.

Generation and receiving side active power (MW)					
Case A					
B1	B4 (r_{o_1})	B5	B8 (r_{o_2})	B9	B12 (r_{o_3})
−1.02	687.6	971.9	625.5	971.9	584
Case B					
B1	B4 (r_{o_1})	B5	B8 (r_{o_2})	B9	B12 (r_{o_3})
−1.02	804.6	971.9	575.5	971.9	484

were performed using MATLAB as a simulation tool. As discussed in Section 1, in comparison with the previous work of [5–13] for load flow balancing and [20] for transient stability analysis, this paper is built on a more general system model in which the impact of more severe three phase faults, i.e., MITPFs, is discussed. The problem under study is new and different from all previous ones. As a result, the proposed algorithm cannot be directly compared with the algorithms presented in [5–13,20]. To overcome this difficulty, we employ two alternative algorithms, one for an SITPF and one for an MITPF in order to clearly illustrate the difference between the effect of these two faults on a power system for load flow balancing and transient stability analysis. Before discussing the algorithms, we first explain why a smart node is a good representation of an electrical network in terms of load flow balancing. This is done through comparison of our approach with the previous approach in [8].

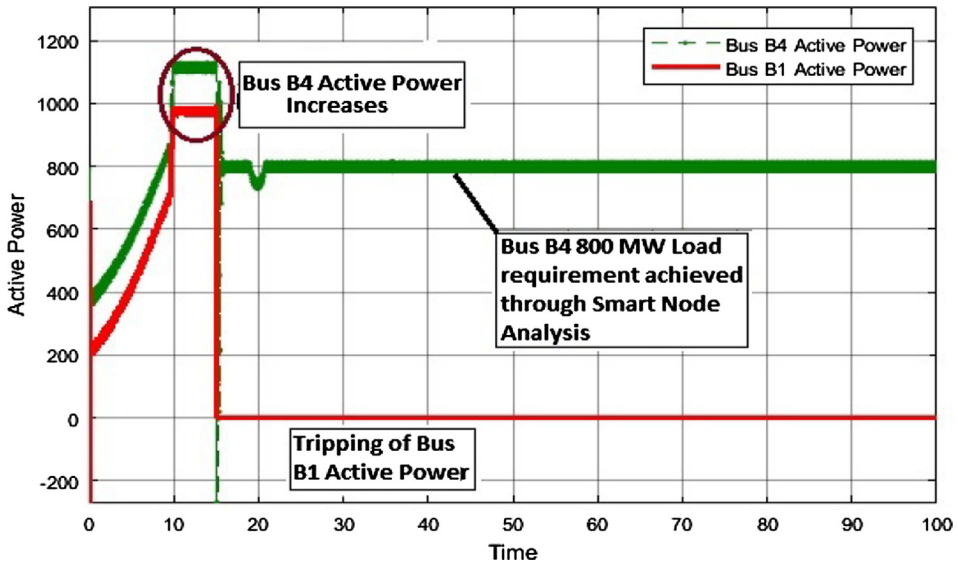

Fig. 9. Buses B1 and B4 active power graphs (SITPF).

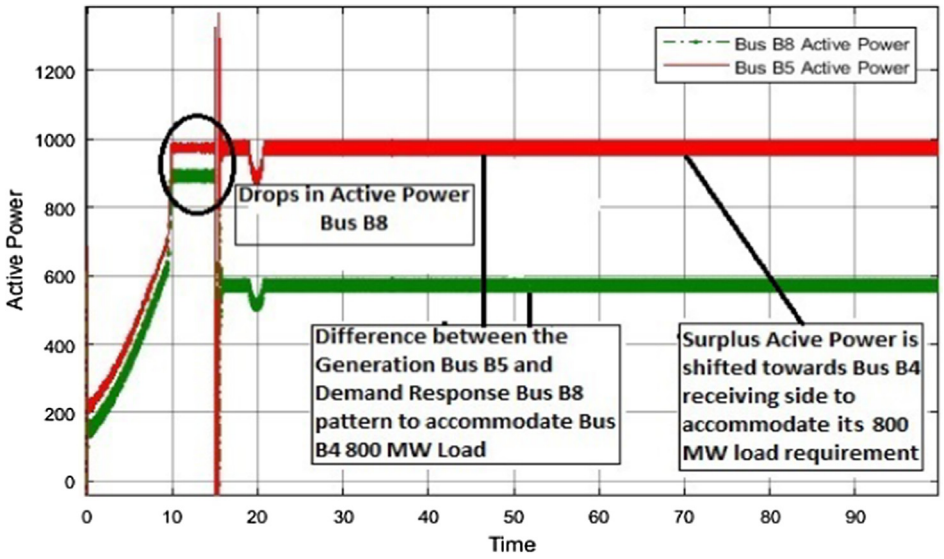

Fig. 10. Buses B5 and B8 active power graphs (SITPF).

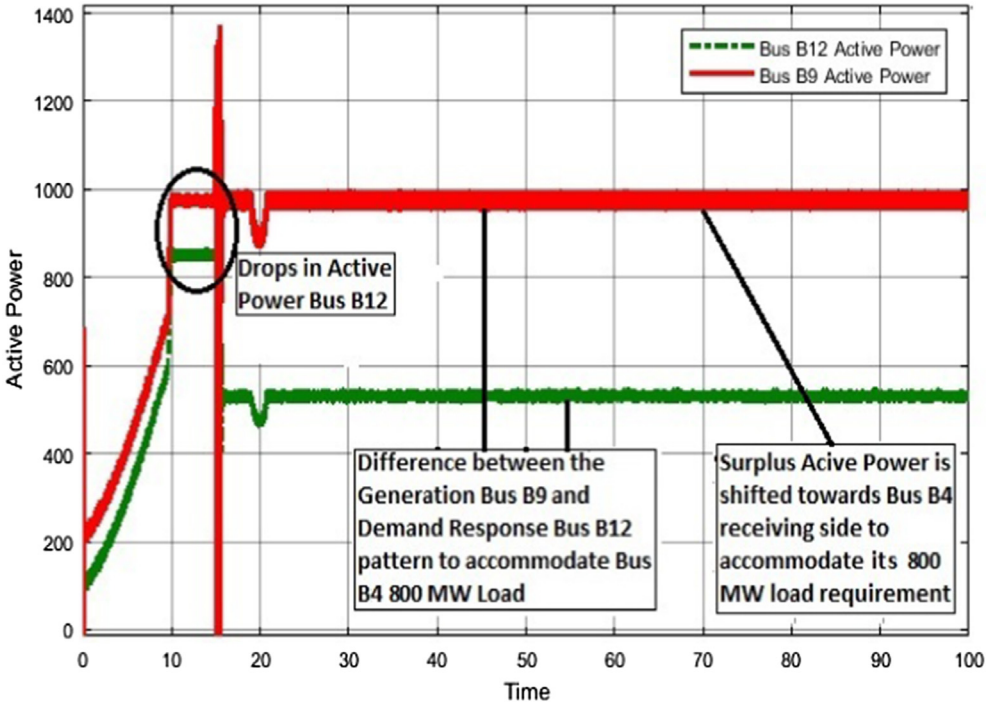

Fig. 11. Buses B9 and B12 active power graphs (SITPF).

To demonstrate that the proposed methods in [5–13] are computationally expensive and the optimal solution for load flow balancing is not guaranteed, considering larger deviations between loads, i.e., from KW to MW, a power system proposed in [8] is examined. The main objective of [8] is to minimize the overall cost of energy imported from the public grid, i.e.,

$$\int_0^T P_i(t)C(t)dt \rightarrow minimize, \tag{44}$$

where, $P_i(t)$ represents the active power supplied from the bus into the power grid, i.e., positive for the generator and negative for the load. Here, $C(t)$ is the price signal ("$"/$MW$), which is a time varying function. The main problem formulated in [8] is to determine the energy/storage function, $E(t)$, that minimizes the main objective function (44). Using (44), the cost function $V(\cdot)$ can be expressed as,

$$V(t, E) = \int_0^T P_i(t)C(t)dt \rightarrow minimize. \tag{45}$$

The objective function in (44) is equivalent to minimizing $V(0, 0)$ in (45), i.e., to reduce the overall cost over the entire period, starting with an empty storage $E = 0$. In this scenario, the optimal solution is to compute recursively using the Bellman equation, i.e.,

$$V(t, E) = \min_{E(t+dt)} \{\Delta V(E, E(t + dt)) + V(t + dt, E(t + dt))\}, \tag{46}$$

which allows solution via backward recursion. This starts at the final time $t = T$, where the cost function is $V(T, E) = 0$. Applying (46), the cost function can be computed at $T-dt$, finding $V(T-dt, E)$ over all the energy values. The process continues until reaching an initial condition, i.e., $t = 0$. A backward recursion step for single storage device is shown in Fig. 2.

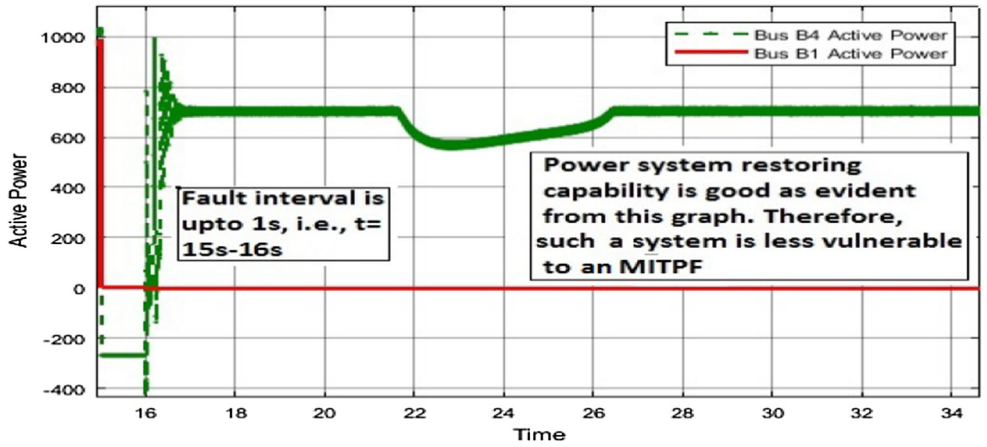

Fig. 12. Buses B1 and B4 active power graphs.

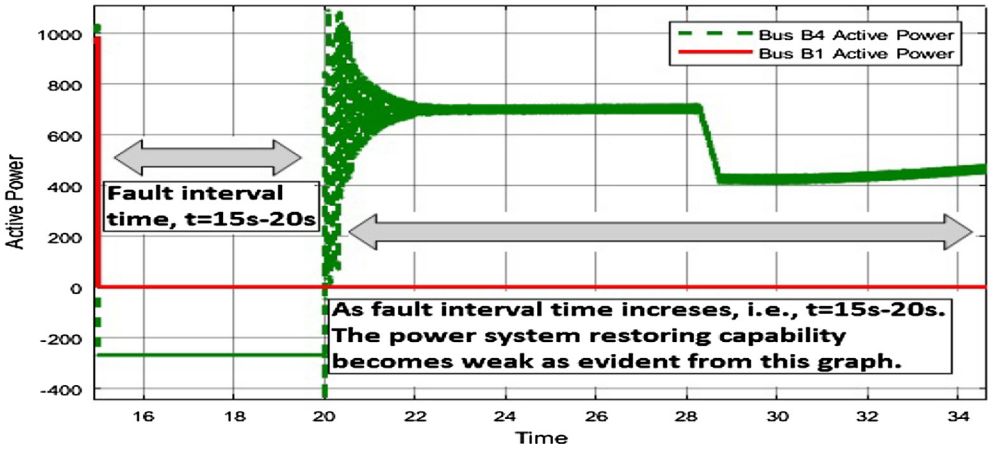

Fig. 13. Buses B1 and B4 active power graphs.

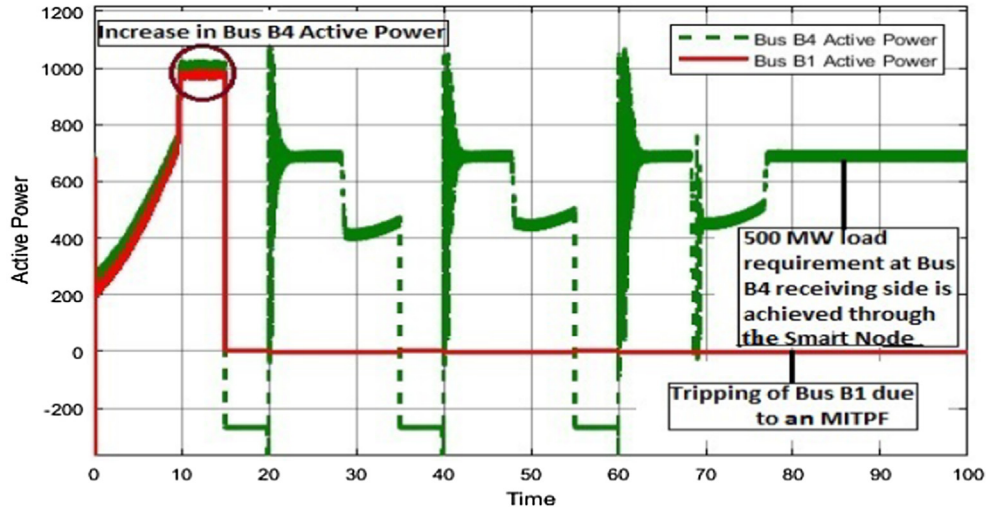

Fig. 14. Buses B1 and B4 active power graphs (MITPF).

Similarly, the same procedure follows if we consider another storage device. The only difference lies in the fact that each storage device adds a new dimension to the solution space. Therefore, an electrical network with two storage devices is a two-dimensional (2-D) problem, with two free variables, i.e., $E_i(t)$ and $E_j(t)$. The major difference in the cost function is that it will become multidimensional, i.e.,

$$V(t, E_i, E_j) = \int_0^T P_i(t)C(t),\, dt \rightarrow minimize, \tag{47}$$

where $E_i(t) = E_i$ and $E_j(t) = E_j$ are initial conditions.

Therefore, (46) will become

$$V(t, E_i, E_j) = \min_{E_i(t+dt), E_j(t+dt)} [\{\Delta V(E_i, E_i(t+dt), E_j, E_j(t+dt)\} + \{V(t+dt, E_i(t+dt), E_j(t+dt)\}]. \tag{48}$$

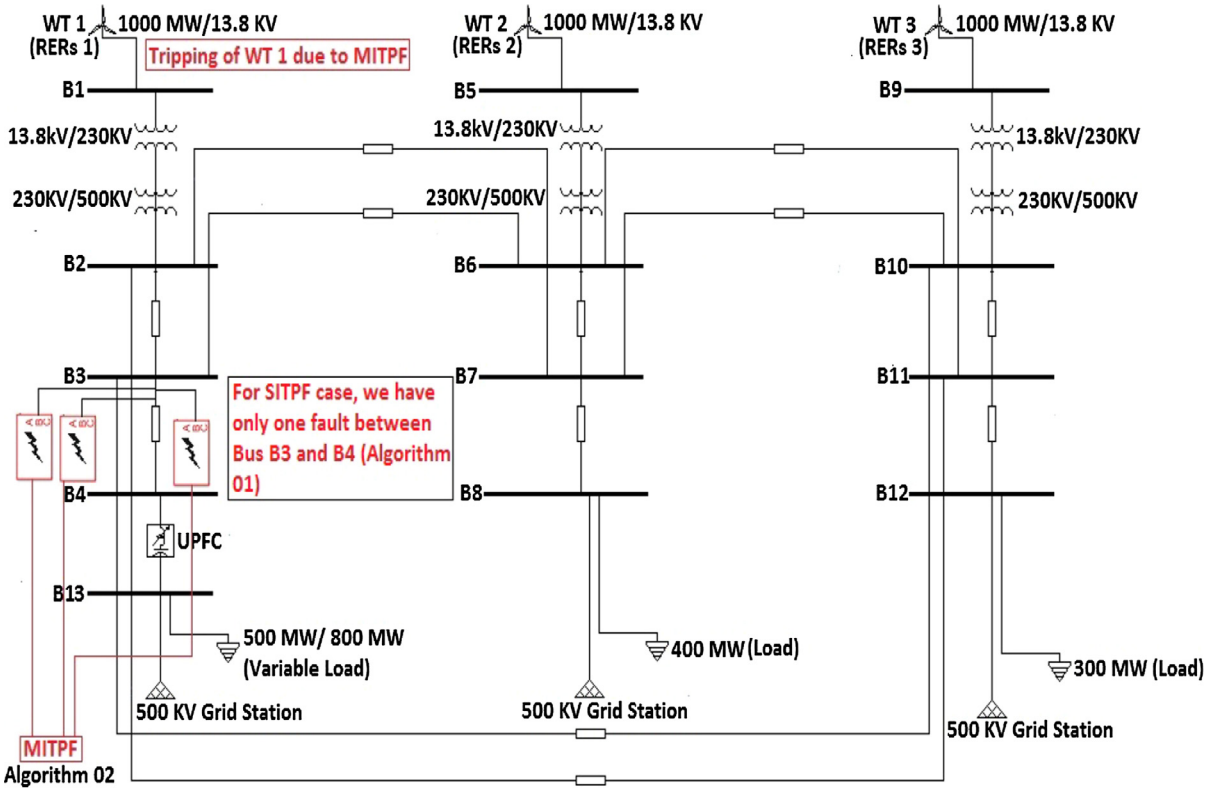

Fig. 15. Smart node and UPFC single line diagram for SITPFs and MITPFs in the power system.

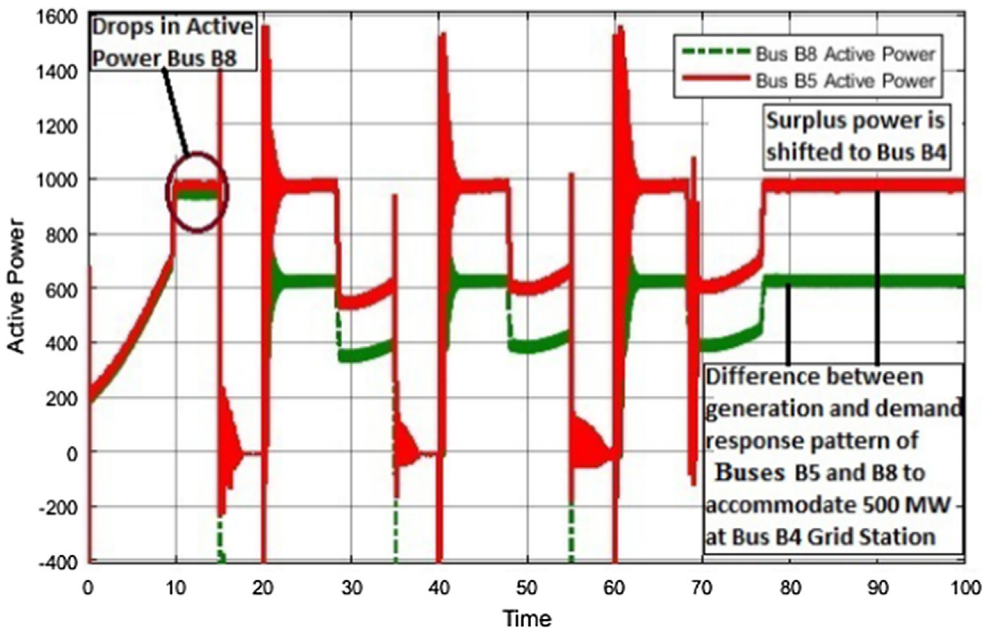

Fig. 16. Buses B5 and B8 active power graphs (MITPF).

A 2-D storage network with a backward recursion process is shown in Fig. 3

The main disadvantage of the approach proposed in [8] is that its numerical complexity increases with the number of storage devices. This is shown in Fig. 3, where the addition of a storage device contributes an extra dimension to the solution space. An electrical network with a single storage device is processed in seconds, even if it contains a large number of buses. However, a power system with four or five storage devices may be evaluated only if it contains just a few buses. Thus, the proposed approach in [8] does not give a practical solution when the integration of different RERs and storage devices into a power system increases, which in turn increases the number of buses. In other words, the proposed approach in [8] is limited to accommodate only smaller loads (KW). Moreover, it is computationally expensive due to the utilization of sophisticated storage devices. Therefore, we propose an entirely new approach, which leads to a totally different solution, and which is capable of circumventing the numerical complexity. Instead of looking at the problem formulated in [8] as minimization of

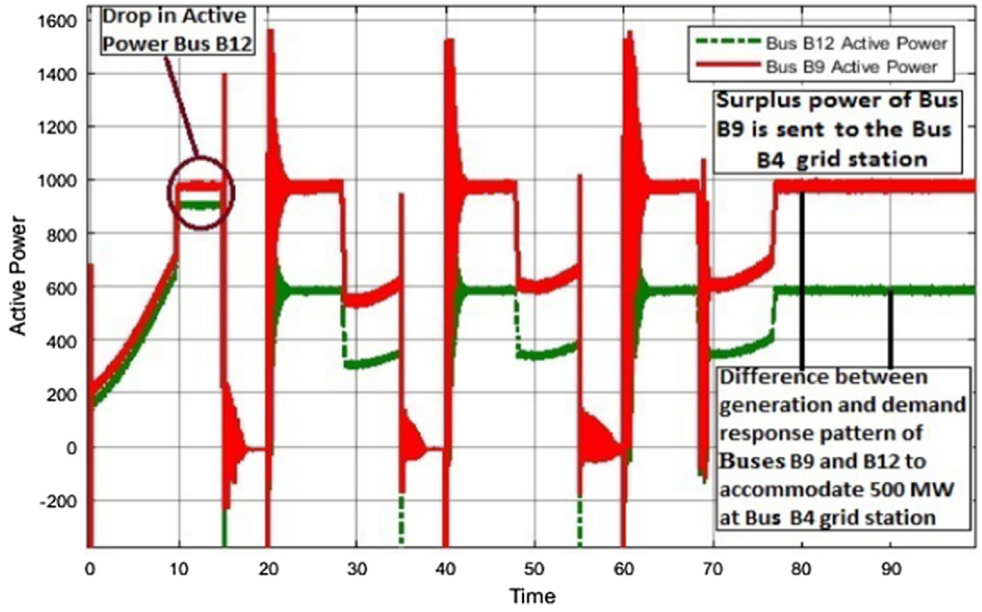

Fig. 17. Buses B9 and B12 active power graphs (MITPF).

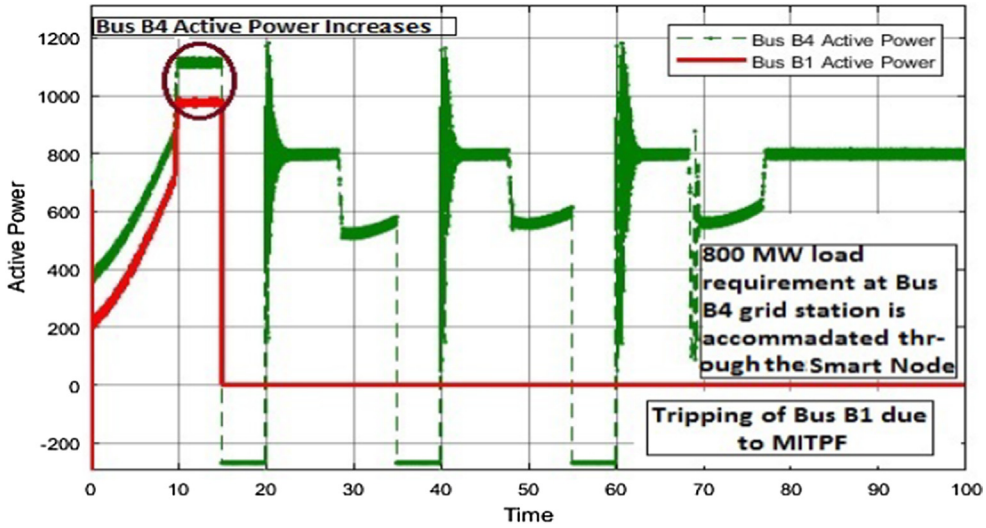

Fig. 18. Buses B1 and B4 active power graphs (MITPF).

costs within constraints and using a small number of RERs and storage devices in order to accommodate smaller loads (KW), we integrate a large number of RERs in the form of a smart node transmission network and use it as a resource to be allocated to different power grid stations. Instead of a cost minimization problem in our proposed work, we consider it as an allocation problem, where power is allocated to accommodate heavy loads (MW) to optimize power imported from different RERs.

3.1. Single interval three phase (L-L-L) fault (Algorithm 1)

Fig. 4 shows the scale-free topological representation of a smart node electrical network. This type of representation is very important when assessing random error related risks, since a random disturbance at any node may relate to one of low connectivity degree. In probabilistic terms, those nodes with fewer connections are most likely to disturb the network. Due to this strong interconnectivity among nodes, we provide an autonomous power flow control between each node and its corresponding power grid station, without considering dedicated transmission nodes.

A smart node basically represents a strong interconnection between different transmission substations/buses in order to provide optimum load flow balancing in the RIPG as shown in Fig. 5. These interconnections between different transmission substations/buses and generators face numerous challenges to accommodate the integration of a high penetration of RERs in terms of achieving an optimum load flow balancing in the RIPG as proposed in [34]. Power system flexibility, or the ability of a power system to meet changes in load demands through utilizing RERs, is one such issue receiving much attention. Considering the reliability issues associated with RERs, a more realistic assessment of a power system's flexibility in terms of load flow balancing can be made. For this purpose, interconnections between different transmission substations/buses in the form of a smart node transmission network can provide a significant contribution to optimum load flow balancing, considering the risk posed to the power system by RERs, in terms of its reliability, especially in the case of an occurrence of an SITPF or MITPF.

Moreover, addressing the variability of RERs for load flow balancing and transient stability in an RIPG, the smart node transmission network will also require an additional level of quick-response control strategies

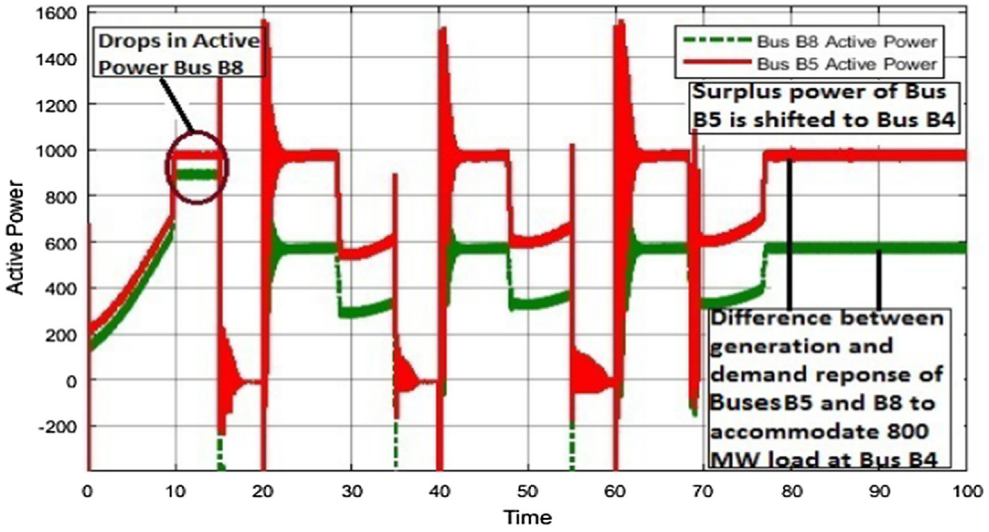

Fig. 19. Buses B5 and B8 active power graphs (MITPF).

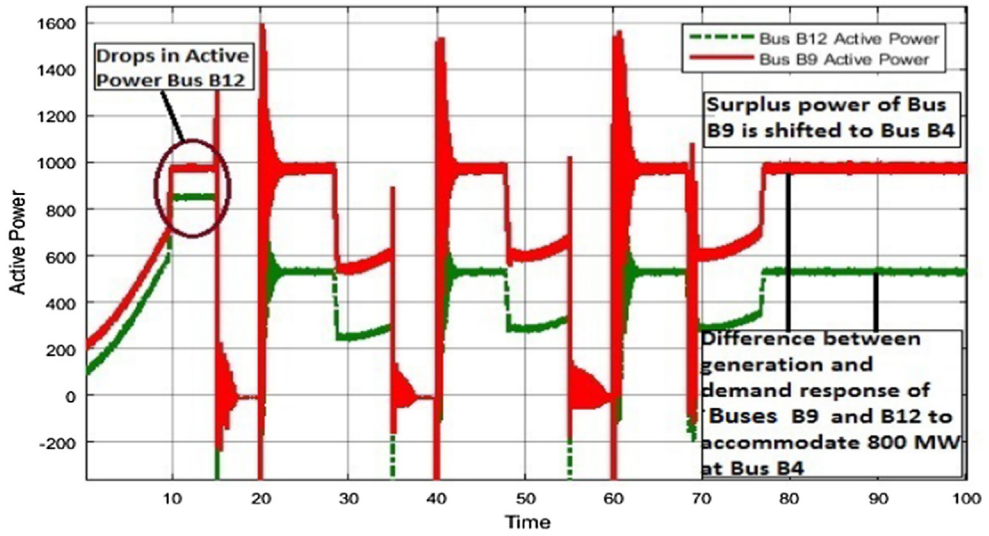

Fig. 20. Buses B9 and B12 active power graphs (MITPF).

in the form of a UPFC to circumvent critical situations. These situations become more severe in the presence of disturbances, i.e., occurrence of an MITPF, where the interactions among different RERs in the form of a smart node for optimum load flow balancing become even more complex.

For load flow balancing, two different case scenarios are considered in order to show the effectiveness of a smart node in a power system due to occurrence of an SITPF. Case-A: loads of $D_1^f(t) = 500$ MW, $D_2^f(t) = 400$ MW and $D_3^f(t) = 300$ MW are required for the power grid stations. Case-B: the load requirement of RER 1's receiving power grid station increases to $D_1^f(t) = 800$ MW. The results of these two cases verify the effectiveness of utilizing a smart node in a power system.

Table 2
Active power on different buses.

Generation and receiving side active power (MW)					
Case A					
B1	B4 (r_{o1})	B5	B8 (r_{o2})	B9	B12 (r_{o3})
−1.02	687.6	971.9	625.5	971.9	584
Case B					
B1	B4 (r_{o1})	B5	B8 (r_{o2})	B9	B12 (r_{o3})
−1.02	802.8	980.9	576.3	980.9	534.7

3.1.1. Case A

Due to reliability issues involving with the RERs, an unexpected SITPF has occurred between buses B3 and B4, in a power system having three wind generating resources as shown in Fig. 15, at a time interval of (15 s–15.1 s), which causes the tripping of the generation resource near bus B1 at $t = 15$ s. This is evident from Fig. 6 (bus B1 active power). Due to tripping of the first RER, its $G_1^a(t) = 0$ MW, while its required forecast supply should be $G_1^f(t) = 500$ MW. Therefore, we have to increase the actual supply to the forecast supply, i.e., $G_1^a(t) = G_1^f(t)$, in order to adjust our forecast demand requirement of $D_1^f(t) = 500$ MW, in terms of its synchronous stability with $G_1^f(t)$. This can be done through a smart node transmission network. Here, the smart node is an intelligent interconnection of the transmission network that will adjust the load requirement of tripping bus B1 of RER 1 by shifting the power from the other two RERs, whose actual supplies are

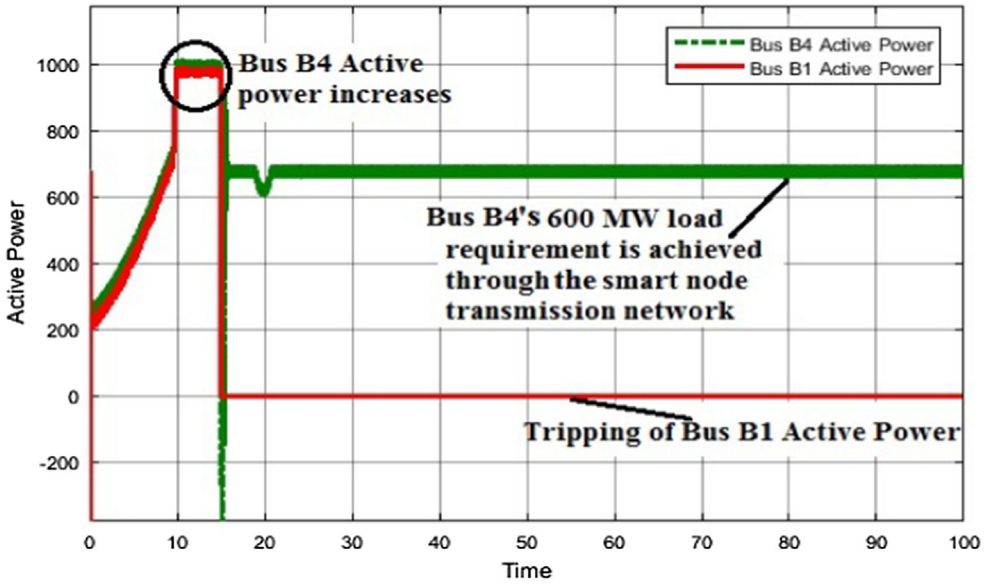

Fig. 21. Buses B1 and B4 active power graph (SITPF).

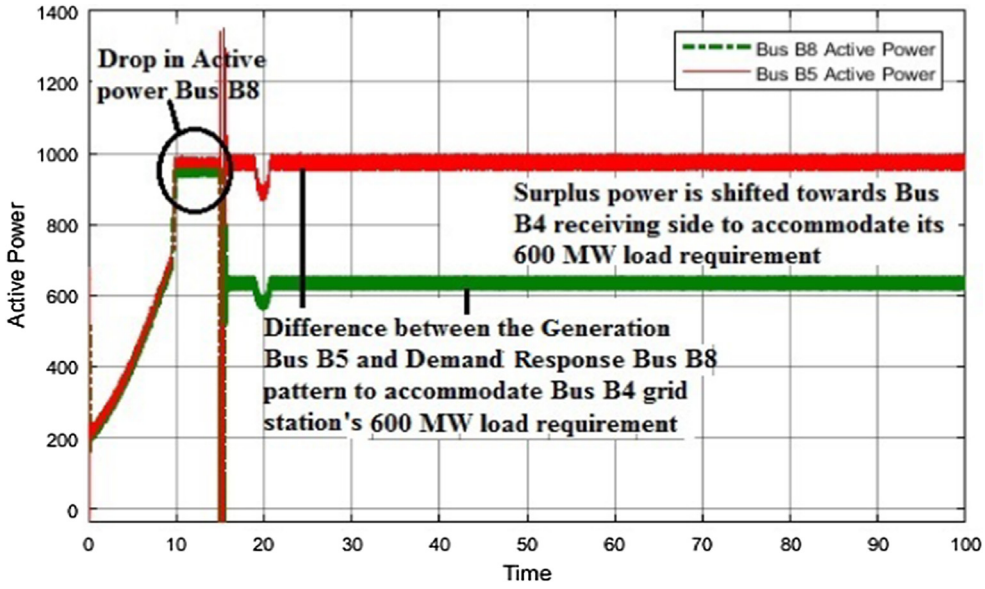

Fig. 22. Buses B5 and B8 active power graphs (SITPF).

$G_2^a(t) = 971.9$ MW and $G_3^a(t) = 971.9$ MW, while its forecast demands are $D_2^f(t) = 400$ MW and $D_3^f(t) = 300$ MW. Therefore, surplus power of RER 2 $(G_2^a(t)-D_2^f(t))$ and RER 3 $(G_3^a(t)-D_3^f(t))$ is shifted to accommodate the forecast demand of 500 MW required of the first power grid station, with corresponding tripping its RER 1 as shown in Figs. 6–8.

In this scenario, we have $r_1(t) = 500\,MW$, $r_2(t) = 400\,MW$ and $r_3(t) = 300$ MW for the three RERs, i.e., reserve $r(t)$ requirements in terms of $D_1^f(t)$, $D_2^f(t)$ and $D_3^f(t)$. The nominal reserve r_o for the three RERs to compensate $r(t)$ are $r_{o_1} = 687.6$ MW, $r_{o_2} = 625.5$ MW and $r_{o_3} = 584$ MW as shown in Table 1. Therefore, $R_G(t)$ for load flow in case of an SITPF for the three RERs are $r_{o1}-r_1(t) = 687.6-500 = 187.6$ MW, $r_{o2}-r_2(t) = 625.5-400 = 225.5$ MW and $r_{o3}-r_3(t) = 584-300 = 284$ MW.

3.1.2. Case B

This case is similar to case-A, the only difference lies in the load requirement on the receiving power grid station with the tripping RER, due to the SITPF. Suppose that the forecast load requirement of the first receiving power grid station correspondingly increases from $D_1^f(t) = 500$ MW to $D_1^f(t) = 800$ MW. In order to compensate the remaining 300 MW of forecast supply, i.e., $G_1^f(t) = 300$ MW, we integrate the RERs into a smart node transmission network so as to accommodate the load adjustment in terms of synchronization between $G_1^f(t)$ and $D_1^f(t)$. The actual supply and forecast demands of RER 2 and RER 3 do not change. Therefore, by considering the same scenario as discussed in case-A, the surplus power of RER 2, i.e., $(G_2^a(t)-D_2^f(t))$ and RER 3, i.e., $(G_3^a(t)-D_3^f(t))$ is shifted to accommodate the 800 MW load requirement of RER 1 as shown in Figs. 9–11.

Similarly, for case-B, we have $r_1(t) = 800$ MW, $r_2(t) = 400$ MW and $r_3(t) = 300$ MW and $r_{o_1} = 804.6$ MW, $r_{o_2} = 575.5$ MW and $r_{o_3} = 484MW$ as shown in Table 1. Therefore, $r_{o_1}-r_1(t) = 804.6-800 = 4.6$ MW, $r_{o_2}-r_2(t) = 575.5-400 = 175.5$ MW and $r_{o_3}-r_3(t) = 484-300 = 184$ MW. As the load requirement of the tripping RER 1 increases from 500 MW to 800 MW, r_{o_1} approaches $r_1(t)$, thereby, minimizing $R_G(t)$. This shows the importance of the smart node to reduce $R_G(t)$ in case of an increasing load requirement in order to achieve synchronous stability between $G^f(t)$ and $D^f(t)$.

Table 1 shows the active power on different buses of the generation

Fig. 23. Buses B9 and B12 active power graphs (SITPF).

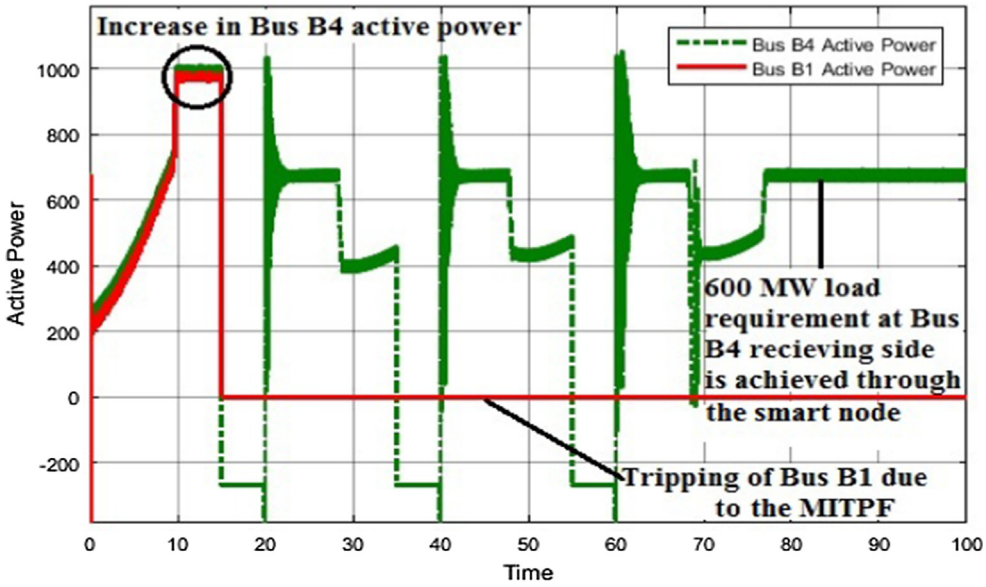

Fig. 24. Buses B1 and B4 active power graphs (MITPF).

and receiving sides. Due to the smart node transmission network topology, the active power on the receiving side is automatically balanced, in terms of its load requirement. The forecast demand requirements of buses B4, B8 and B12 in case-A for the SITPF should be $D_1^f(t) = 500$ MW, $D_2^f(t) = 400$ MW and $D_3^f(t) = 300$ MW, while the forecast demand requirements in case-B should be $D_1^f(t) = 800$ MW, $D_2^f(t) = 400$ MW and $D_3^f(t) = 300$ MW. This can be achieved through the smart node for both cases, as is evident from the receiving side buses, i.e., (B4, B8, B12) from the below Table 1.

3.2. Multiple interval three phase (L-L-L) fault analysis (Algorithm 02)

To investigate the effects of MITPFs on power systems, a realistic scenario is considered, which causes the circuit breaker to open and close at multiple time slots. An example of such a scenario is lightning striking a transmission line at multiple time intervals causing an MITPF in the power system. When an MITPF occurred between bus B3 and B4 at time intervals, $t_1 = 15$ s–20 s, $t_2 = 45$ s–50 s and $t_3 = 65$ s–70 s, it caused the tripping of wind turbine 1 near bus B1 as shown in Fig. 14 and Fig. 15. Due to the MITPF, the circuit breaker is opened and closed at multiple time slots, i.e., opened at $t_1 = 15$ s, $t_2 = 45$ s and $t_3 = 65$ s and closed at $t_1 = 20$ s, $t_2 = 50$ s and $t_3 = 70$ s. Due to these multiple closings and opening of the circuit breaker, power quality issues arise in terms of multiple transients and power dispatchability. The power system vulnerability assessment in case of an MITPF is verified through simulation results. For this purpose, two case scenarios were considered. In the first case, the fault duration is up to 1 s, i.e., $t = 15$ s–16 s as shown in Fig. 12. In the second case, the fault occurrence time is up to 5 s, i.e., $t = 15$ s–20 s as shown in Fig. 13. In this second case, the three phase (L-L-L) fault is sustained for a certain interval of time. It will degrade the power grid restoring capability after closing of the circuit breaker, i.e., at $t = 20$ s. This makes the power system potentially vulnerable to the MITPF.

An MITPF was simulated upto three intervals to show its effects on the system as shown in Figs. 14, 16 and 17. Again, the load flow balancing can be done through a smart node transmission network. In

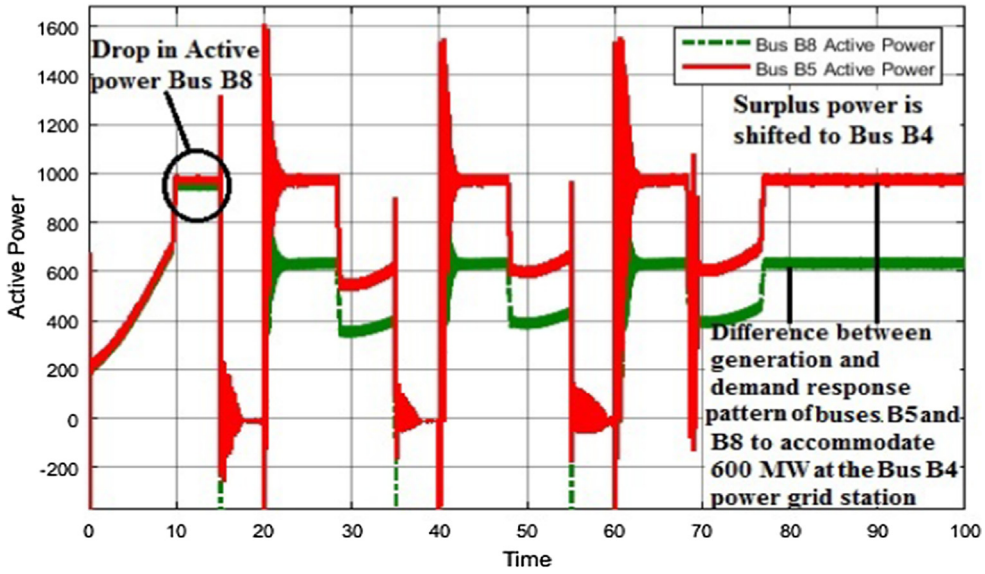

Fig. 25. Buses B5 and B8 active power graphs (MITPF).

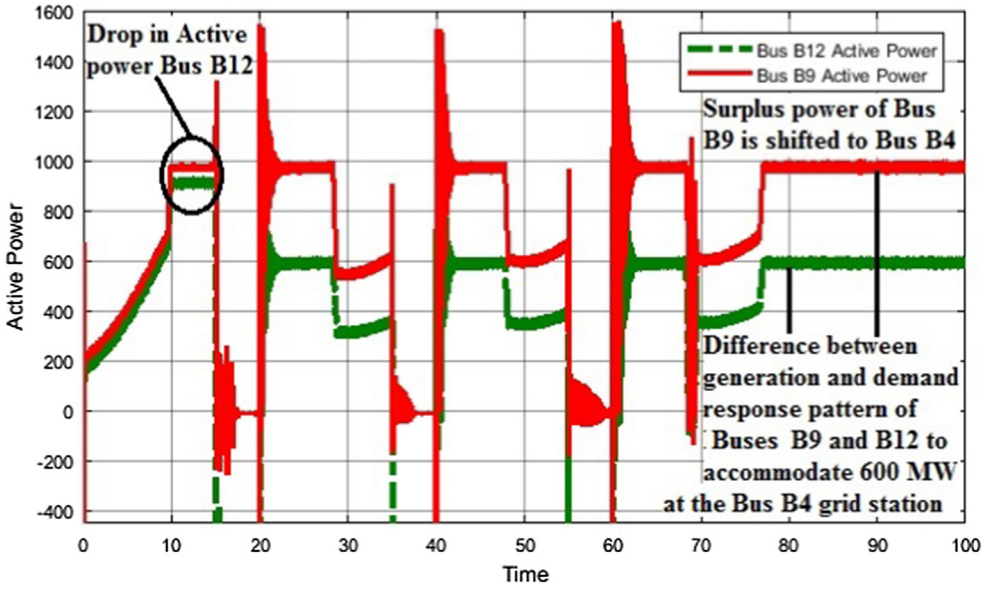

Fig. 26. Buses B9 and B12 active power graphs (MITPF).

Table 3
Active power on different buses.

Generation and receiving side active power (MW)					
Case A (SITPF)					
B1	B4 (r_{o_1})	B5	B8 (r_{o_2})	B9	B12 (r_{o_3})
−1.01	680.1	982.2	638.9	982.2	597.6
Case B (MITPF)					
B1	B4 (r_{o_1})	B5	B8 (r_{o_2})	B9	B12 (r_{o_3})
−1.01	678.4	979.3	637.1	979.3	595.7

order to analyze the effectiveness of the smart node for load flow balancing during an MITPF, similar case scenarios are considered, as were discussed for an SITPF (Algorithm 1).

3.2.1. Case A

The MITPF near RER 1 between buses B3 and B4 causes the tripping of the wind turbine near bus B1 as shown in Figs. 14 and 15, with a corresponding load requirement of $G_1^f(t) = 500$ MW. Therefore, in order to accommodate the receiving grid station of RER 1, a load requirement of each power grid station was adjusted according to its required load by using the smart node transmission network topology. It is clearly illustrated from Figs. 16 and 17 that due to the low load requirements, i.e., $D_2^f(t) = 400$ MW and $D_3^f(t) = 300$ MW, at receiving grid stations 2 and 3, their extra generating power, i.e., $(G_2^a(t) - D_2^f(t))$ and $(G_3^a(t) - D_3^f(t))$ is shifted towards the receiving grid station of RER 1. This is done to accommodate the $G_1^f(t) = 500MW$ requirement of RER 1's power grid station as shown in Fig. 14. The randomness $R_G(t)$ in the MITPF is the same as in case-A for the SITPF.

3.2.2. Case B

Similarly, consider the same load requirement of RER 1's power grid station as considered in case-B for the SITPF, i.e., an increasing load requirement from 500 MW to 800 MW. Therefore, in order to

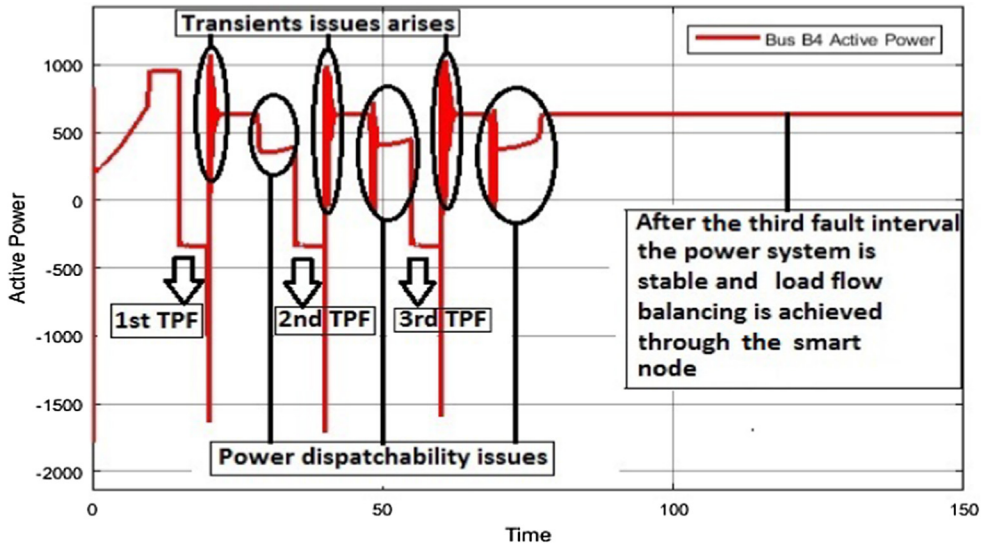

Fig. 27. Bus B4 active power graph (MITPF).

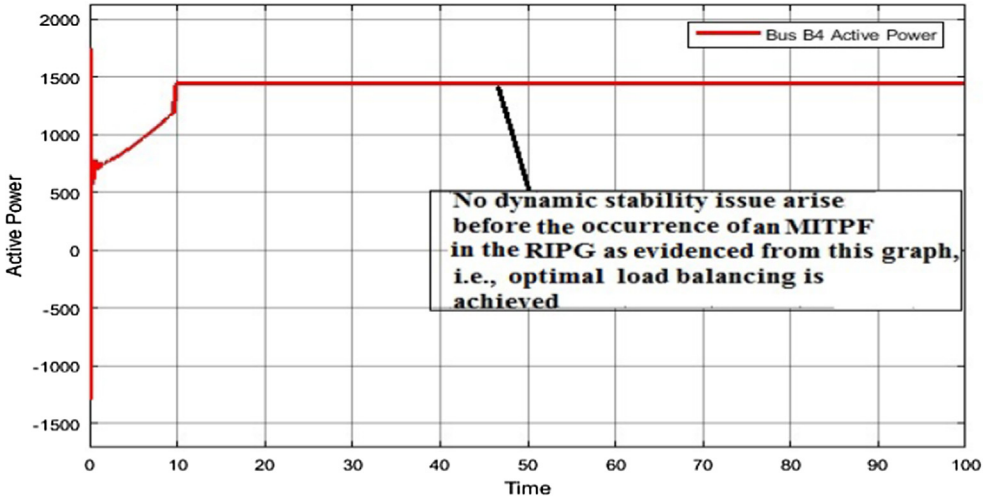

Fig. 28. No dynamic stability issues arise in terms of the active power graph before the occurrence of an MITPF in the RIPG.

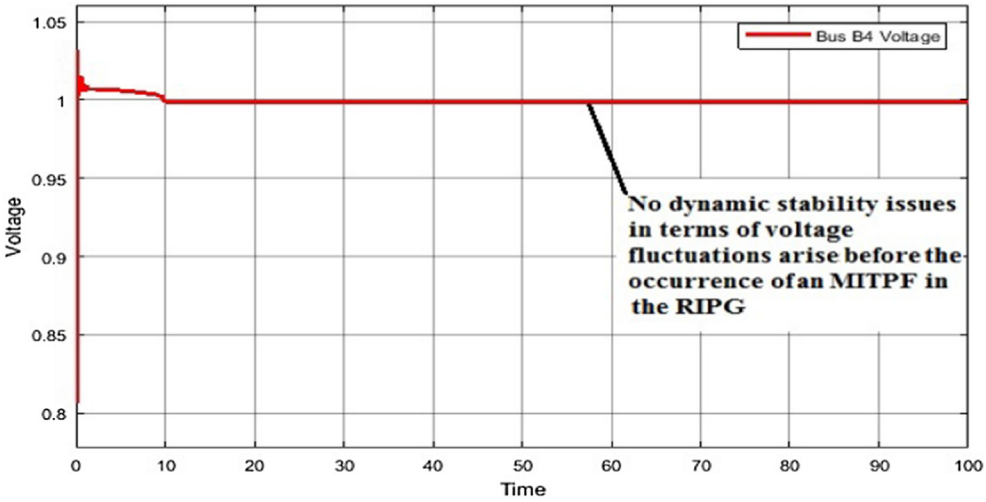

Fig. 29. No dynamic stability issues arise in terms of the voltage graph before an occurrence of MITPF in the RIPG.

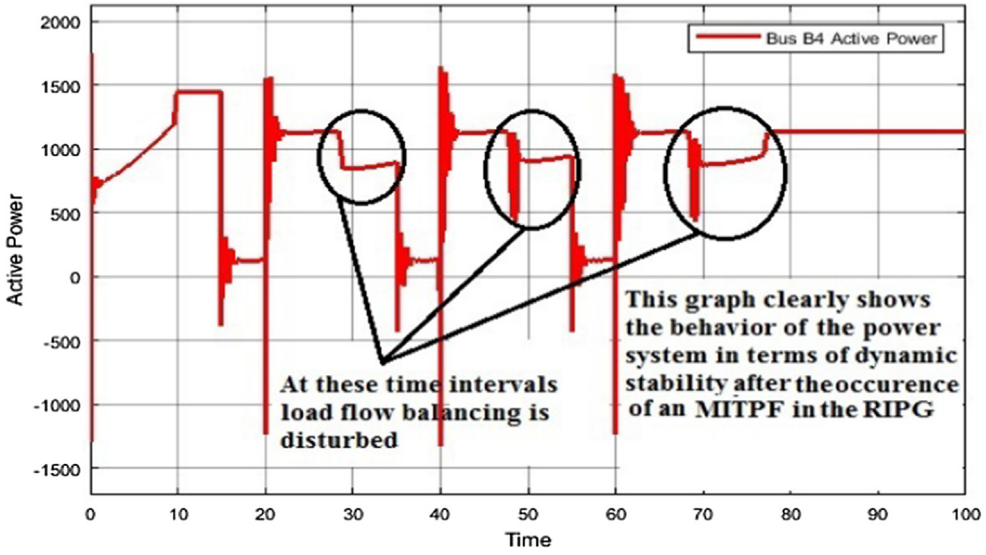

Fig. 30. Dynamic stability issues arise in terms of the active power graph after an occurrence of an MITPF in the RIPG.

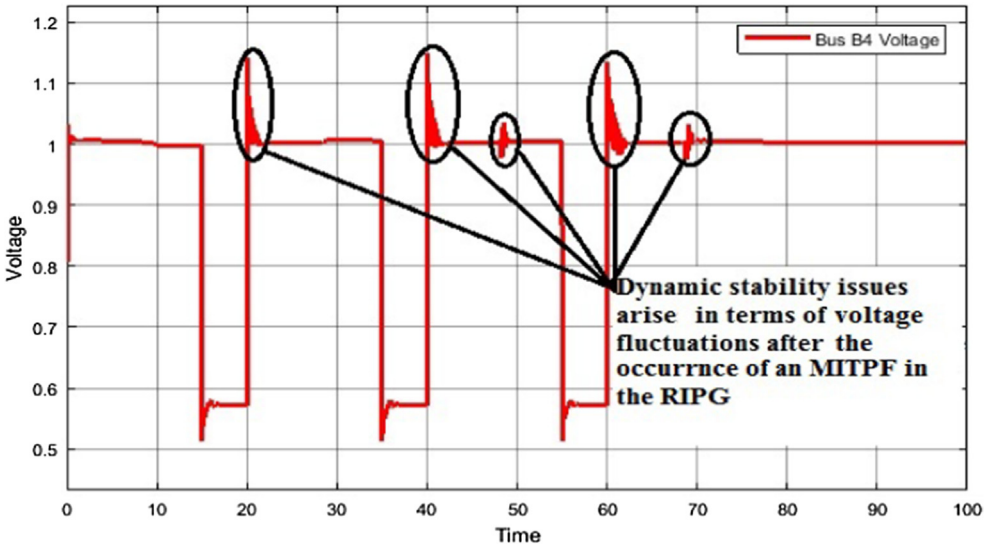

Fig. 31. Dynamic stability issues arise in terms of the voltage graph after an occurrence of an MITPF in the RIPG.

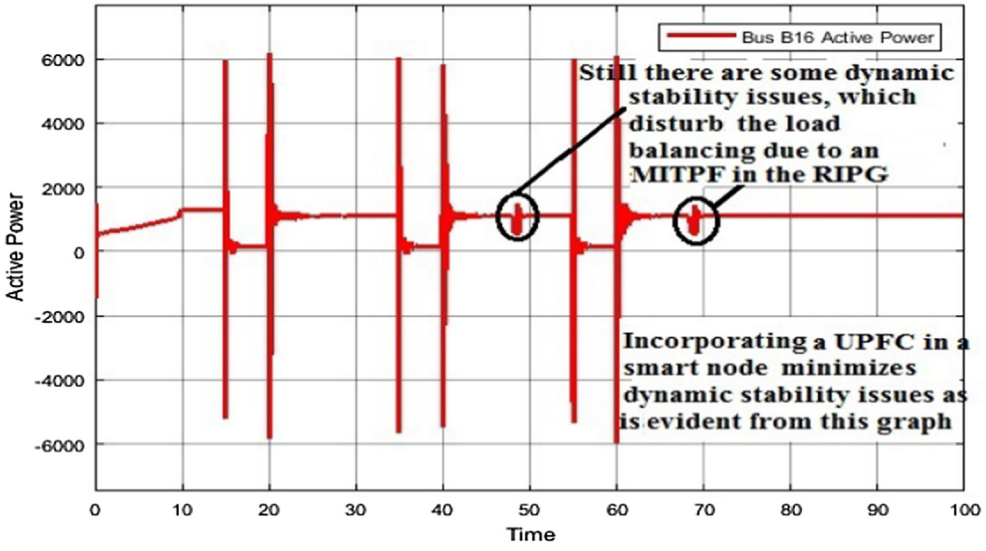

Fig. 32. Reducing dynamic stability issues by using a UPFC in the case of an occurrence of an MITPF in the RIPG (active power graph).

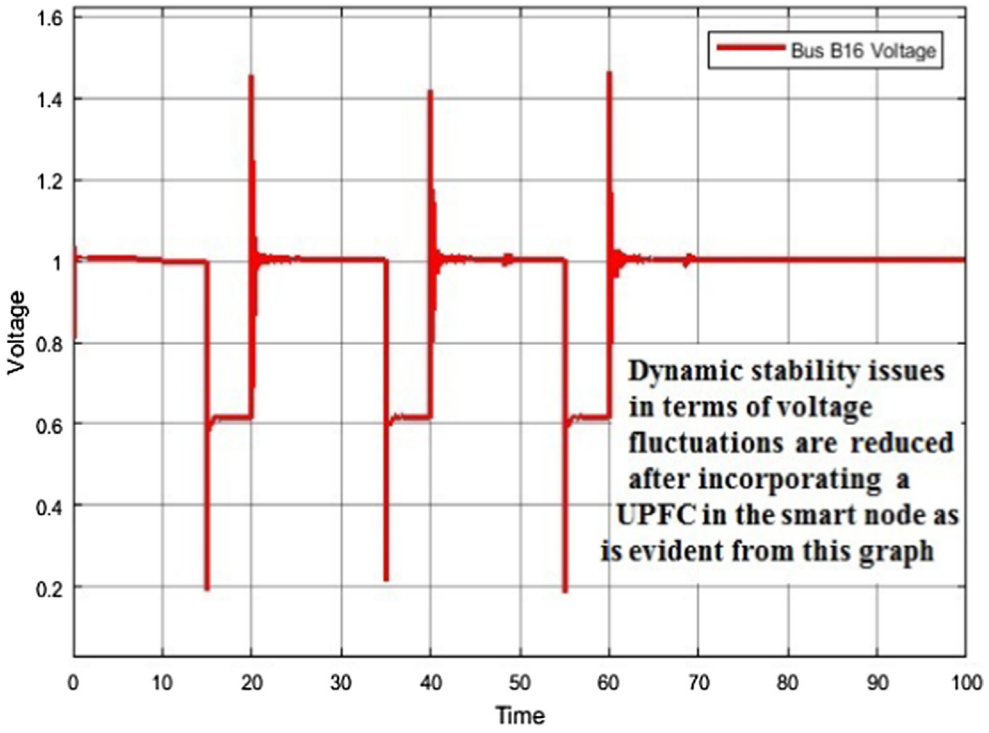

Fig. 33. Reducing dynamic stability issues by using a UPFC in the case of an occurrence of an MITPF in the RIPG (voltage graph).

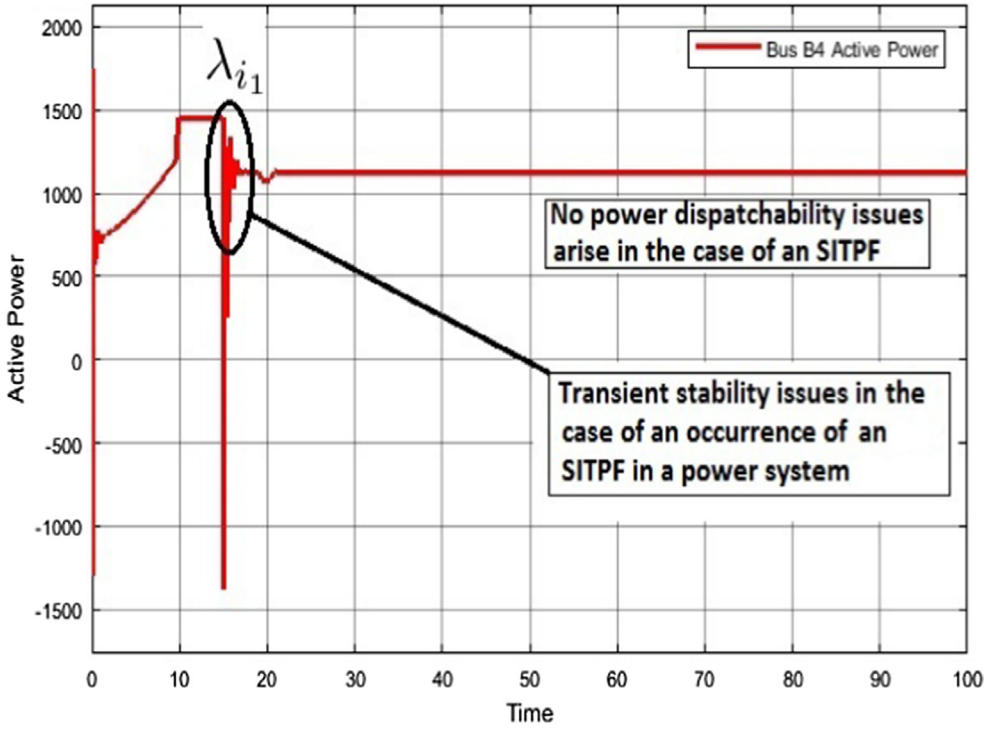

Fig. 34. Bus B4 active power graph without the UPFC (SITPF).

accommodate the $D_2^f(t) = 800$ MW load, more power is shifted from receiving grid stations 2 and 3, whose load requirements are low, i.e., $D_2^f(t) = 400$ MW and $D_3^f(t) = 300$ MW towards the receiving power grid station 1 of RER 1. This can be done through the smart node transmission network, as clearly illustrated from Figs. 18–20.

$R_G(t)$ for the three RERs in this case is determined using the same approach as discussed in case-B for the SITPF, i.e., $R_{G_1}(t) = 2.8$ MW, $R_{G_2}(t) = 176.3$ MW and $R_{G_3}(t) = 134.7$ MW. Table 2 shows that in spite of outages of 500 MW and 800 MW at receiving grid station 1 in both cases, due to tripping of RER 1 at $t = 15$ s, i.e., $G_1^a(t) = 0$ MW, the active power on the receiving side is still balanced according to the load requirements between the three grid stations. The forecast demand requirements of buses B4, B8 and B12 in case-A of the MITPF should be $D_1^f(t) = 500$ MW, $D_2^f(t) = 400$ MW and $D_3^f(t) = 300$ MW. While their forecast demand requirements in case-B should be $D_1^f(t) = 800$ MW, $D_2^f(t) = 400$ MW and $D_3^f(t) = 300$ MW.

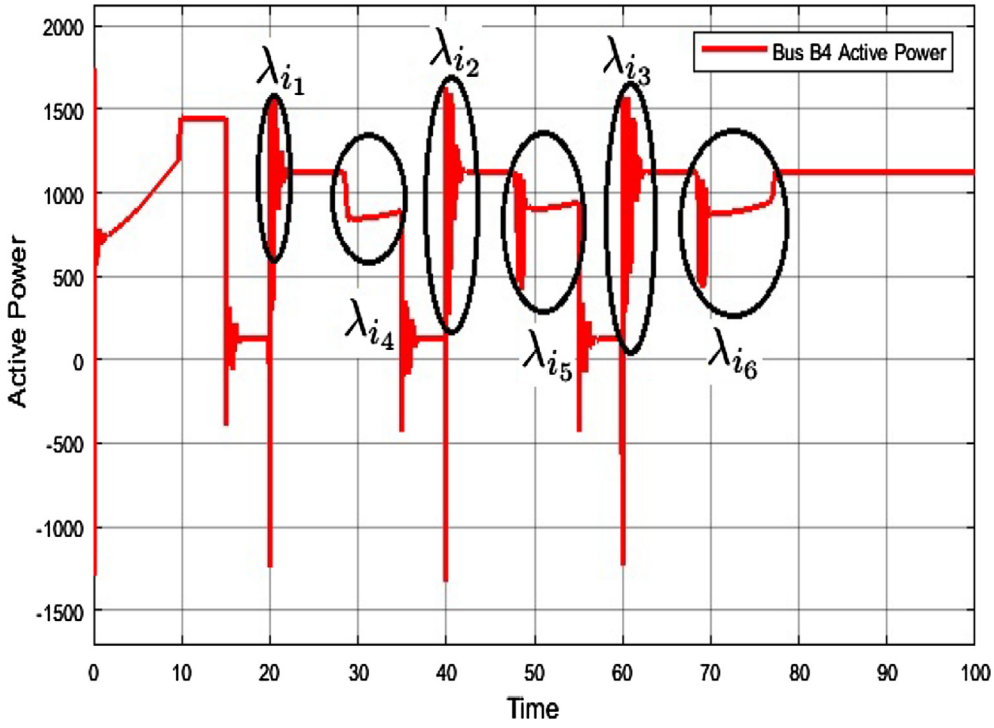

Fig. 35. Bus B4 active power graph without the UPFC (MITPF).

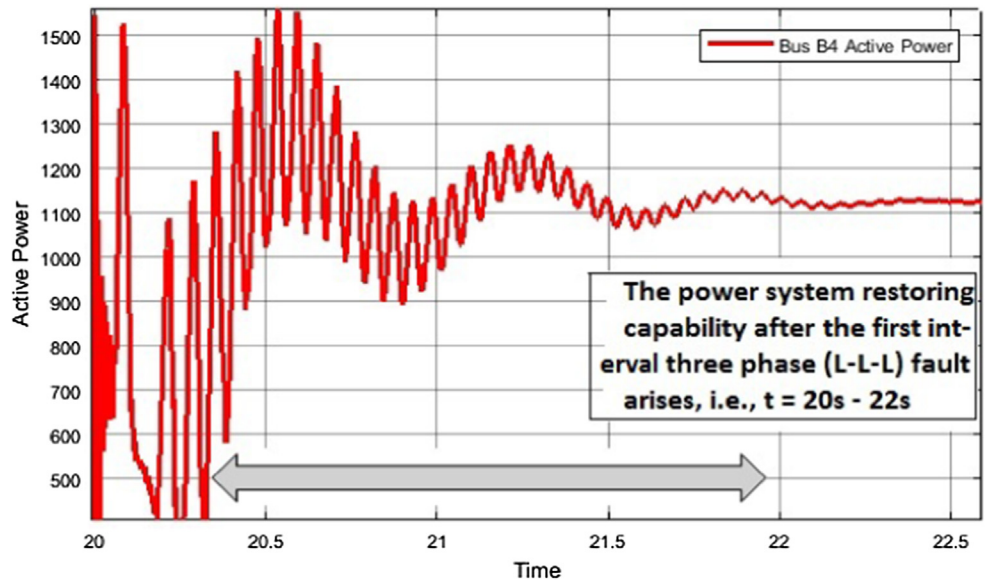

Fig. 36. First interval fault transient stability analysis.

This can be done through the smart node transmission network for both the cases, as evident from the receiving side buses, i.e., (B4, B8, B12) from Table 2.

3.3. Load flow balancing in the case of heavier loads in the RIPG (SITPF or MITPF)

This case scenario is similar to previous cases, the only difference lies in the forecast load requirement $D^f(t)$ of each receiving side power grid station, i.e., instead of utilizing 500 MW/800 MW (variable load) at receiving power grid station 1, and 400 MW and 300 MW (constant load) at receiving power grid stations 2 and 3, we consider heavier loads, i.e., 600 MW, 500 MW and 400 MW at receiving power grid stations 1, 2 and 3, respectively. In this case scenario, the smart node transmission network still optimizes the load flow at the receiving side of the RIPG. Figs. 21–23 show an optimum load flow balancing through the smart node in case of an occurrence of an SITPF in the RIPG (case-A). Whereas, considering the scenario of an MITPF in the RIPG, a further larger load requirements is still achievable by utilizing the smart node as shown in Figs. 24–26 (case-B).

Table 3 shows that in spite of an outage of 600 MW load at receiving power grid station 1 due to the tripping of RER 1 at $t = 15$ s, i.e., $G_1^a(t) = 0$ MW, the active power on the receiving side is still balanced according to load requirements between the three grid stations. The forecast requirements for buses B4, B8 and B12 in case-A for an SITPF and case-B for an MITPF should be $D_1^f(t) = 600$ MW, $D_2^f(t) = 500$ MW and $D_3^f(t) = 400$ MW. This can be done through the smart node transmission network for both cases and it is clearly evident from the

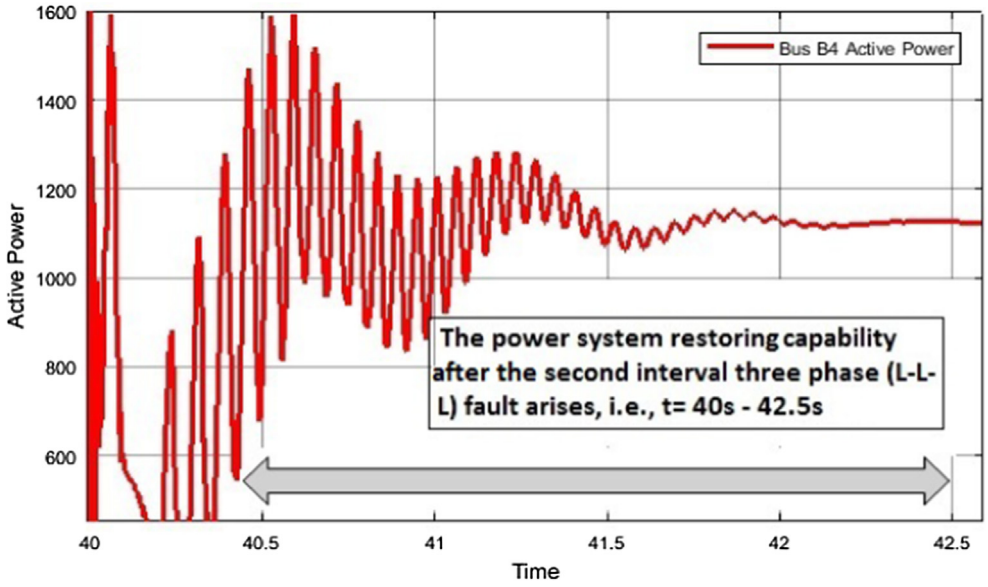

Fig. 37. Second interval fault transient stability analysis.

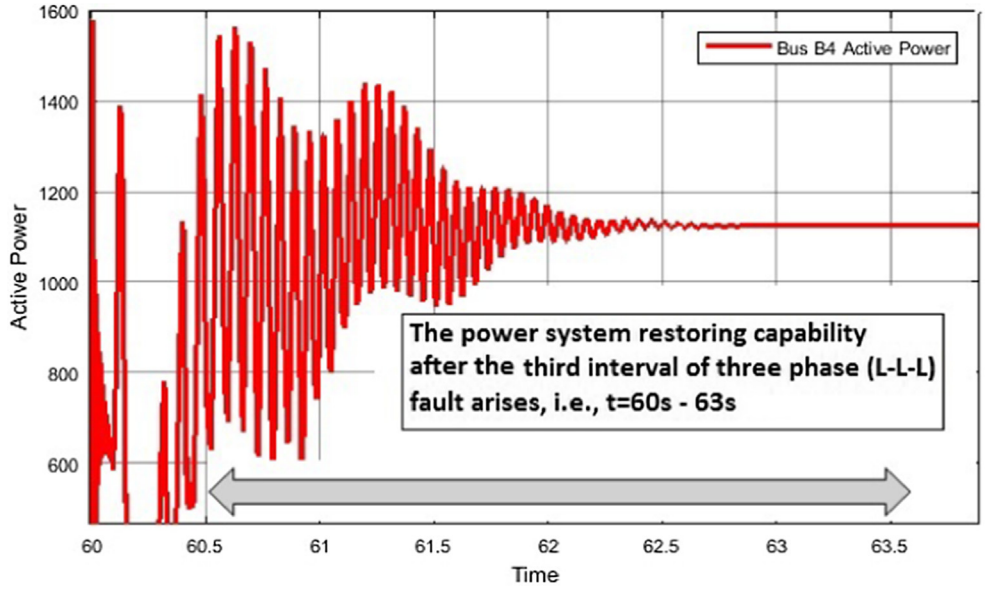

Fig. 38. Third interval fault transient stability analysis.

receiving side buses, i.e., (B4, B8, B12) from Table 3. For case-A (SITPF), we have $r_1(t) = 600$ MW, $r_2(t) = 500$ MW and $r_3(t) = 400$ MW and $r_{o_1} = 680.1$ MW, $r_{o_2} = 638.9$ MW and $r_{o_3} = 597.6$ MW as shown in Table 3. Therefore, $R_G(t)$ is given by $R_{G_1}(t) = r_{o_1} - r_1(t) = 680.1 - 600 = 80.1$ MW, $R_{G_2}(t) = r_{o_2} - r_2(t) = 638.9 - 500 = 138.9$ MW and $R_{G_3}(t) = r_{o_3} - r_3(t) = 597.6 - 400 = 197.6$ MW. Similarly, for case-B (MITPF), we have $r_1(t) = 600$ MW, $r_2(t) = 500$ MW and $r_3(t) = 400$ MW and $r_{o_1} = 678.4$ MW, $r_{o_2} = 637.1$ MW and $r_{o_3} = 595.7$ MW as shown in Table 3. Therefore, $R_G(t)$ is, i.e., $R_{G_1}(t) = r_{o_1} - r_1(t) = 678.4 - 600 = 78.4$ MW, $R_{G_2}(t) = r_{o_2} - r_2(t) = 637.1 - 500 = 137.1$ MW and $R_{G_3}(t) = r_{o_3} - r_3(t) = 595.7 - 400 = 195.7$ MW.

From Fig. 27, it can be noticed that there are still issues of multiple transients and power dispatchability after each fault interval due to closing and opening of the circuit breaker at multiple time slots in the case of an MITPF. This causes deviations between $D^f(t)$ and $G^f(t)$. Therefore, a UPFC should be incorporated into a smart node transmission network to overcome these power quality disturbances and further optimize the power system for load flow balancing. Moreover, in order to explain the necessity of a UPFC in the smart node transmission network, we consider a scenario of occurrence of an MITPF in the RIPG with respect to dynamic stability analysis in the next section.

3.4. Dynamic stability analysis in the RIPG

Dynamic stability can be defined as the stability of a power system during and after sudden changes or disturbances due to short-circuits, loss of generators, sudden changes in load, line tripping, or any other similar impacts as proposed in [35,36]. Here, our main aim is to investigate the impact of three phase (L-L-L) faults based on single or multiple intervals on power system stability in the context of an RIPG. Therefore, we consider the issue of dynamic stability with respect to occurrence of an SITPF or MITPF in the RIPG and investigate their effects on power system stability before and after occurrence of these faults. In order to verify load flow balancing in term of dynamic stability, we have performed further simulations. We focus on the occurrence of an MITPF, as single interval faults have been considered

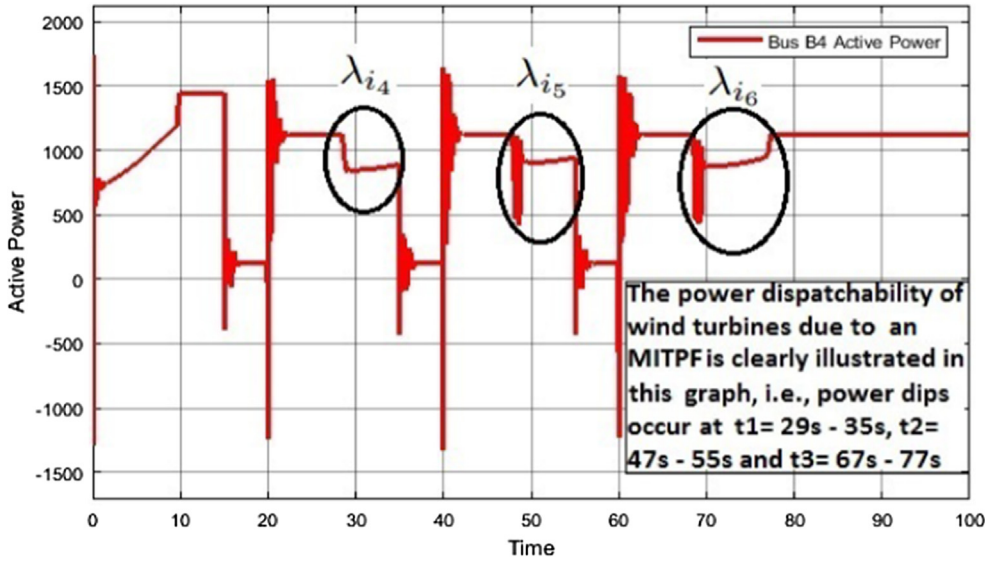

Fig. 39. Bus B4 active power graph without the UPFC (MITPF).

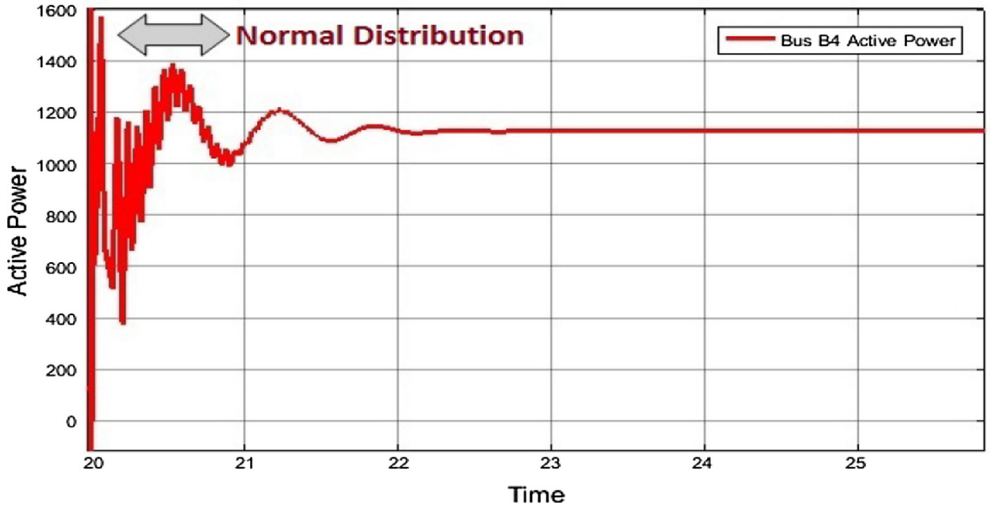

Fig. 40. Normal distribution pattern for transient delays.

extensively in this context in the literature.

The dynamic stability of a power system is mainly controlled by the generators. Thus, if conventional synchronous generators are replaced with wind turbine generators having variable speed operational systems, the dynamic stability of the power will be significantly affected. Therefore, there is a need to equip the power system with FACTS devices, i.e., UPFCs, in order to compensate the effects on dynamic stability of the power system, especially in those case scenarios when the power generated by renewable energy resources exceeds that of conventional synchronous generators. Therefore, in our case scenario incorporation of a UPFC in the smart node transmission network is necessary to completely optimize the RIPG for load flow balancing through minimizing dynamic stability issues. This scenario is further verified by simulation results in terms of active power transients and voltage fluctuations as shown in Figs. 28 and 29 before occurrence of an MITPF in the RIPG and Figs. 30 and 31 after occurrence of an MITPF in the RIPG. Moreover, the compensation of these dynamic stability issues in the RIPG using the UPFC and the importance of incorporating the UPFC into the smart node transmission network is clearly illustrated through Figs. 32 and 33.

Considering dynamic stability analysis in the RIPG, it is clear that there is a need to equip the RIPG with a UPFC in the case of an occurrence of an MITPF. In order to clarify the effects of an MITPF on the RIPG based on each fault interval, and its compensation requirements, the transient fault analysis behavior of an RIPG in case of occurrence of an MITPF using a UPFC is discussed in the next section.

3.5. Transient fault analysis during multiple interval three phase (L-L-L) faults using UPFC

Fig. 15 shows a schematic of a sixteen bus system having three renewable energy (wind) generating resources, with each having generating capacity of 1000 MW, that are interconnected in the form of a smart node. Considering the vulnerability assessment of MITPFs in power systems as discussed in Section 3.2, an unexpected outage, in terms of an MITPF has occurred between buses B3 and B4, as shown in Fig. 15. Now, to improve the power dispatchability and reliability of the power grid, the UPFC has been put into operation between buses B4 and B13 as shown in Fig. 15. Based on the effects of the MITPF on the power system, the influence of the UPFC in terms of transient stability is analyzed. More importantly, first the effects of the MITPF on the power system is analyzed for power quality disturbances, with respect to an SITPF and its power quality effects on the power system as already proposed in [20]. Then, the effectiveness of the UPFC is analyzed for

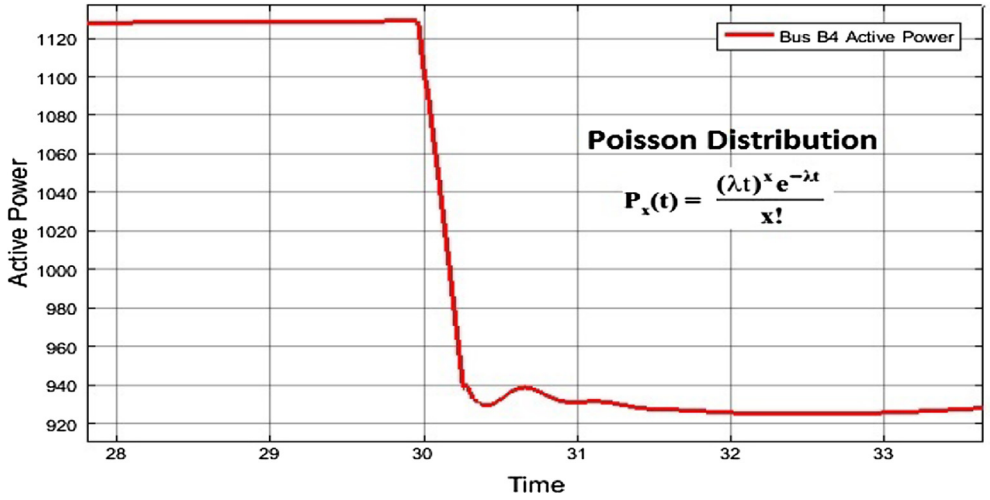

Fig. 41. Poisson distribution pattern for power dip delays.

reducing the multiple transient and power dispatchability issues due to the MITPF.

3.5.1. Effect of transients and power dips

Fig. 35 illustrates the effects of transients, with corresponding delays of λ_{i_1}, λ_{i_2} and λ_{i_3}, and power dispatchability with delays of λ_{i_4}, λ_{i_5} and λ_{i_6}, due to the occurrence of an MITPF on a synchronized transmission network, when no UPFC is incorporated between buses B4 and B13, as shown in Fig. 15. The differences between the effect of the proposed MITPF scheme and the already discussed SITPF in [20] for power system reliability, in terms of transients and power dispatchability, is clearly illustrated in Figs. 34 and 35. Fig. 34 shows that only single transients arise with corresponding delay of λ_{i_1}, while no power dispatchability issues arise in the case of an SITPF. Whereas, with an MITPF as shown in Fig. 35, multiple delays arise due to multiple transients, i.e., λ_{i_1}, λ_{i_2} and λ_{i_3}, and multiple power dispatchability issues, i.e., λ_{i_4}, λ_{i_5} and λ_{i_6}.

An comprehensive analysis of Fig. 35 shows that due to opening and closing of the circuit breaker at multiple time slots with corresponding fault intervals, the power quality issues in terms of transients and power dispatchability are increased, due to the MITPF. This is evident from Figs. 36–38 at timing intervals of $t_1 = 20$ s–22 s (delay upto 2 s), $t_2 = 40$ s–42.5 s (delay upto 2.5 s) and $t_3 = 60$ s–63 s (delay upto 3 s), which correspond to transient levels, and Fig. 39 at $t_1 = 29$ s–35 s (delay upto 6 s), $t_2 = 47$ s–55 s (delay upto 8 s) and $t_3 = 67$ s–77 s (delay upto 10 s) that correspond to power dip levels, as previously discussed in Algorithm 1. This arising of significant oscillations in the RIPG is due to the occurrence of the MITPF. As we already discussed, that due to the occurrence of an MITPF, it will degrade the power system restoring capability after each fault interval as shown in Figs. 36–38. This is due to the opening and closing of the circuit breaker at multiple time slots. Due to these power quality disturbances, a significant oscillation has been observed.

The delays in terms of transients, i.e., λ_{i_1}, λ_{i_2} and λ_{i_3}, and power dips, i.e., λ_{i_4}, λ_{i_5} and λ_{i_6}, are shown in Fig. 35, following the Normal and Poisson distribution patterns, as shown in Figs. 40 and 41.

3.5.2. Transient stability enhancement using a UPFC

These multiple transient and power dispatchability issues due to an MITPF will be fed back in terms of $F(t)$ and returned to the power system as returning demand $B(t)$ as shown in Fig. 1. Therefore, $B(t)$ must be fulfilled in order to keep the system in a stable state. For this

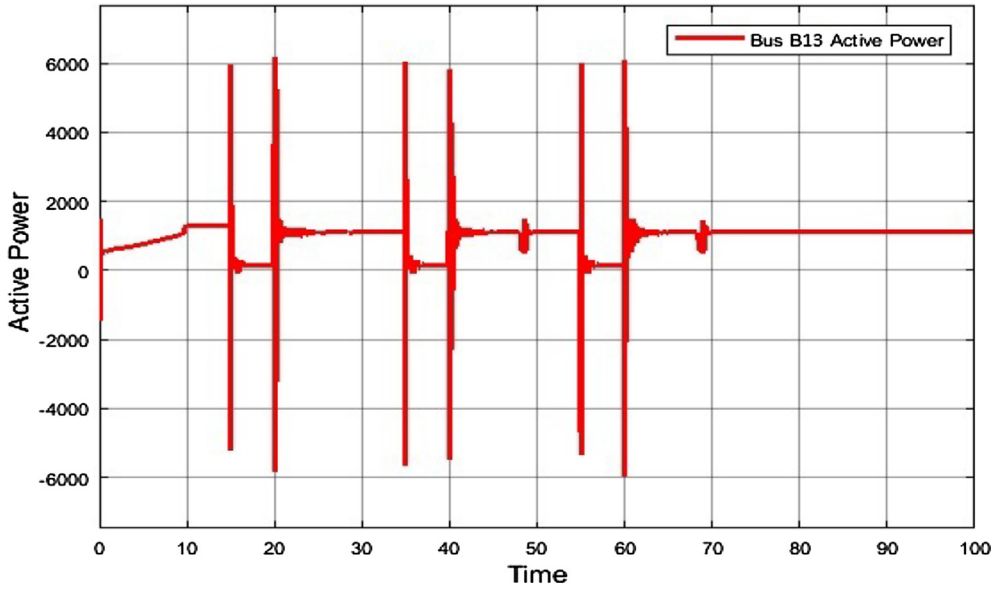

Fig. 42. Bus B4/B13 active power graph with the UPFC (MITPF).

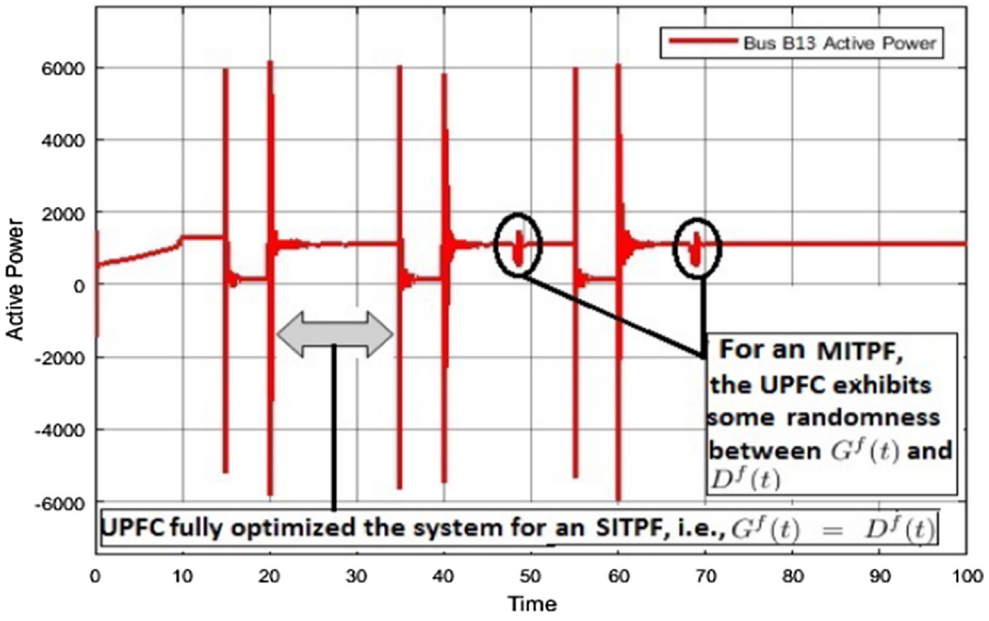

Fig. 43. Bus B4/B13 active power graph with UPFC (MITPF).

purpose, a UPFC should be incorporated into the smart node transmission network in order to control $G(t-1)$ for further optimizing the power system, in order to achieve synchronous stability between $G^f(t)$ and $D^f(t)$. Fig. 42 shows the effects of transient stability enhancement, in terms of active power with the inclusion of a UPFC between buses B4 and B13, as shown in Fig. 15. By comparing Figs. 35 and 42, it is clearly seen that with the inclusion of the UPFC in the smart node transmission network, the load flow balancing through the smart node is further optimized in terms of reducing multiple transients and power dispatchability due to the MITPF in the power system.

In order to effectively investigate the performance of the UPFC in improving the power flow control through the power system network in the case of an MITPF, an comprehensive analysis of Fig. 42 is necessary to validate the simulation results as shown in Fig. 43. From Fig. 43, it can be seen that after the first fault interval (SITPF), the UPFC fully optimizes the power system, i.e., $r_0 = r(t)$. While, in the cases of second and third interval faults (MITPF), there are still some deviations between r_0 and $r(t)$ as shown in Figs. 44 and 45. This shows that after the first fault interval, $F(t)$ in Fig. 1 has been fully compensated using the UPFC, whereas, for the second and third faults, the UPFC compensation is disturbed due to the difference between r_0 and $r(t)$. Recall that $r(t)$ represents the reserve requirement in terms of $D^f(t)$ and r_0 is the nominal reserve in the form of the UPFC. Moreover, the only difference between the UPFC model for the SITPF or MITPF is the contingency time analysis. In case of an SITPF, we have only one contingency issue, due to the single interval fault, while in case of an MITPF, we have multiple contingency issues in terms of multiple transients and power dispatchability.

4. Conclusion

RIPGs are potentially vulnerable to power quality disturbances due

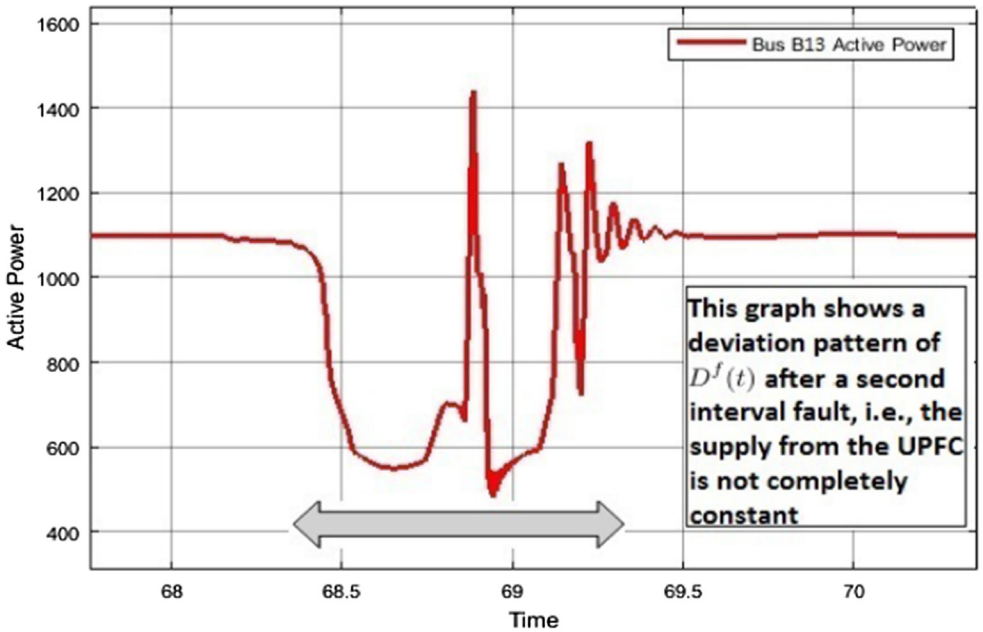

Fig. 44. Second MITPF random deviation pattern.

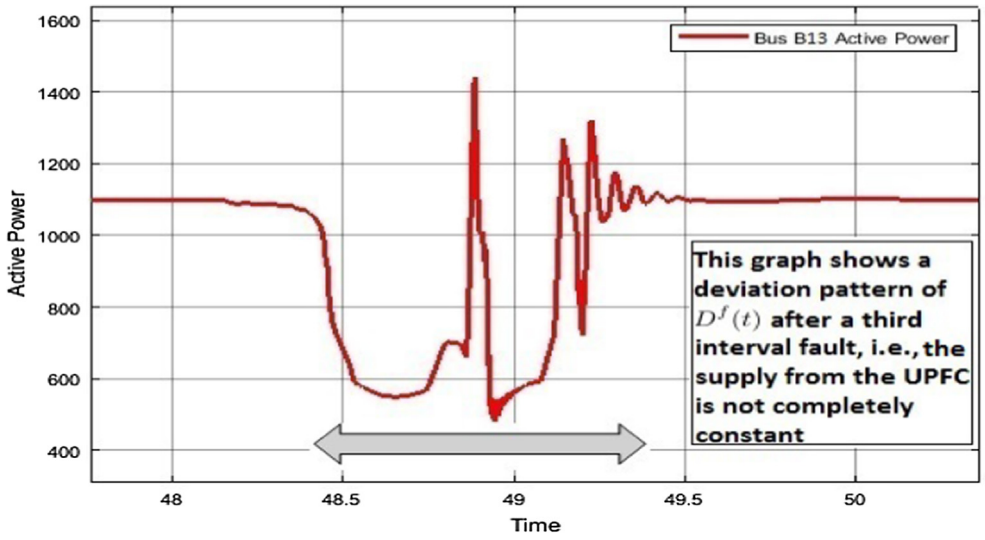

Fig. 45. Third MITPF random deviation pattern.

to congestion and scalability issues. In this paper, probabilistic modeling in terms of a smart node and UPFC has been used to first detect the randomness in a power system, in terms of an occurrence of an SITPF or MITPF. These modeling techniques provide for efficient load flow balancing and lead to reduction in the power dispatchability and transient stability issues on the receiving side of power grid stations, in case of either of SITPFs or MITPFs. The probabilistic modeling significantly improves the accuracy to efficiently reduce future instabilities in power systems due to SITPFs or MITPFs. Moreover, the proposed method allows one to choose the optimal control mode and setting of one UPFC, during an occurrence of an MITPF in a synchronized network of three generating resources. The method can be extended to calculate simultaneously the optimal control mode and settings of multiple UPFC units, in cases of MITPFs.

References

[1] Sato T, Kammen DM, Duan B, Macuha M, Zhou Z, Wu J, Tariq M, Asfaw SA. Smart grid standards: specifications, requirements, and technologies. John Wiley & Sons Singapore Pte. Ltd; 2015. p. 379–93. Ch. Future of the Smart Grid.

[2] Tariq M, Poor HV. Electricity theft detection and localization in grid-tied microgrids. IEEE Trans Smart Grid 2016(99):1–8. https://doi.org/10.1109/TSG.2016.2602660.

[3] Acharya N, Liu CC. Tripping of wind turbines during a system fault. In: Proc. 2008 IEEE power and energy society general meeting – conversion and delivery of electrical energy in the 21st century; 2008. pp. 1–8.

[4] Rajabi-Ghahnavieh A, Fotuhi-Firuzabad M, Shahidehpour M, Feuillet R. UPFC for enhancing power system reliability. IEEE Trans Power Delivery 2010;25(4):2881–90.

[5] Sun S, Dong M, Liang B. Distributed real-time power balancing in renewable-integrated power grids with storage and flexible loads. IEEE Trans Smart Grid 2016;7(5):2337–49. https://doi.org/10.1109/TSG.2015.2445794.

[6] Gill S, Kockar I, Ault GW. Dynamic optimal power flow for active distribution networks. IEEE Trans Power Syst 2014;29(1):121–31. https://doi.org/10.1109/TPWRS.2013.2279263.

[7] Weckx S, Driesen J. Load balancing with EV chargers and PV inverters in unbalanced distribution grids. IEEE Trans Sustain Energy 2015;6(2):635–43. https://doi.org/10.1109/TSTE.2015.2402834.

[8] Levron Y, Guerrero JM, Beck Y. Optimal power flow in microgrids with energy storage. IEEE Trans Power Syst 2013;28(3):3226–34. https://doi.org/10.1109/TPWRS.2013.2245925.

[9] Fan M, Vittal V, Heydt GT, Ayyanar R. Probabilistic power flow analysis with generation dispatch including photovoltaic resources. IEEE Trans Power Syst 2013;28(2):1797–805. https://doi.org/10.1109/TPWRS.2012.2219886.

[10] Aien M, Fotuhi-Firuzabad M, Rashidinejad M. Probabilistic optimal power flow in correlated hybrid wind photovoltaic power systems. IEEE Trans Smart Grid 2014;5(1):130–8. https://doi.org/10.1109/TSG.2013.2293352.

[11] Kabir M, Mishra Y, Bansal R. Probabilistic load flow for distribution systems with uncertain PV generation. Appl Energy 2016;163:343–51. https://doi.org/10.1016/j.apenergy.2015.11.003. URL:http://www.sciencedirect.com/science/article/pii/S0306261915014440.

[12] Wu C, Wen F, Lou Y, Xin F. Probabilistic load flow analysis of photovoltaic generation system with plug-in electric vehicles. Int J Electr Power Energy Syst 2015;64(Complete):1221–8. https://doi.org/10.1016/j.ijepes.2014.09.014.

[13] Chen W, Yan H, Pei X, Wu B. Probabilistic load flow calculation in distribution system considering the stochastic characteristic of wind power and electric vehicle charging load. In: Proc. 2016 IEEE PES Asia-pacific power and energy engineering conference (APPEEC); 2016. p. 1861–66.https://doi.org/10.1109/APPEEC.2016.7779812.

[14] Abdelouahed T, Ahmed ZS. Modeling and transient simulation of unified power flow controllers UPFC in power system. In: Proc. 2015 4th International Conference on Electrical Engineering (ICEE); 2015. pp. 1–7.

[15] Chowdhury MSR, Howlader MM, Hasan AKMK, Ferdaus MR. Distinctive study of UPFC and fault analysis under simulated environment. In: Proc. 2015 Third International Conference on Technological Advances in Electrical, Electronics and Computer Engineering (TAEECE); 2015. pp. 251–255.

[16] Moravej Z, Pazoki M, Khederzadeh M. New pattern-recognition method for fault analysis in transmission line with UPFC. IEEE Trans Power Delivery 2015;30(3):1231–42.

[17] Youssef KH, Abouelenin FM. Analysis of simultaneous unbalanced short circuit and open conductor faults in power systems with untransposed lines and six-phase sections. Alexandria Eng J 2016;55(1):369–77.

[18] Wang L, Li HW, Wu CT. Stability analysis of an integrated offshore wind and seashore wave farm fed to a power grid using a unified power flow controller. IEEE Trans Power Syst 2013;28(3):2211–21.

[19] Novak M, Kravec R, Kanlik M, Conka Z, Kolcun M. UPFC influence to transient stability of power system. In: Proc. 2014 ELEKTRO; 2014. pp. 343–46.

[20] Ananth D, Kumar GN. Fault ride-through enhancement using an enhanced field oriented control technique for converters of grid connected DFIG and STATCOM for different types of faults. ISA Trans 2016;62:2–18. https://doi.org/10.1016/j.isatra.2015.02.014. sI: Control of Renewable Energy Systems.http://www.sciencedirect.com/science/article/pii/S0019057815000749.

[21] Aghaei J, Zarei M, Asban M, Ghavidel S, Heidari A, Agelidis VG. Determining potential stability enhancements of flexible ac transmission system devices using corrected transient energy function. IET Gener Transm Distrib 2016;10(2):470–6. https://doi.org/10.1049/iet-gtd.2015.0849.

[22] Gholipour E, Saadate S. Improving of transient stability of power systems using UPFC. IEEE Trans Power Delivery 2005;20(2):1677–82. https://doi.org/10.1109/TPWRD.2005.846354.

[23] Haque MH. Evaluation of first swing stability of a large power system with various facts devices. IEEE Trans Power Syst 2008;23(3):1144–51. https://doi.org/10.1109/TPWRS.2008.926095.

[24] Qader M. Design and simulation of a different innovation controller-based UPFC (unified power flow controller) for the enhancement of power quality. Energy 2015;89:576–92. https://doi.org/10.1016/j.energy.2015.06.012. URL:http://www.sciencedirect.com/science/article/pii/S0360544215007239.

[25] Kumar NS, Gokulakrishnan J. Impact of facts controllers on the stability of power systems connected with doubly fed induction generators. Int J Electrical Power Energy Syst 2011;33(5):1172–84. https://doi.org/10.1016/j.ijepes.2011.01.031. URL:http://www.sciencedirect.com/science/article/pii/S0142061511000706.

[26] Guo J, Crow ML, Sarangapani J. An improved UPFC control for oscillation damping. IEEE Trans Power Syst 2009;24(1):288–96. https://doi.org/10.1109/TPWRS.2008.2008676.

[27] Jayashri R, Kumudini Devi R. Effect of tuned unified power flow controller to mitigate the rotor speed instability of fixed-speed wind turbines. Renew Energy 2009;34(3):591–6. https://doi.org/10.1016/j.renene.2008.06. URL:https://ideas.repec.org/a/eee/renene/v34y2009i3p591-596.html.

[28] Shojaeian S, Soltani J, Markadeh GA. Damping of low frequency oscillations of multi-machine multi-UPFC power systems, based on adaptive input-output

feedback linearization control. IEEE Trans Power Syst 2012;27(4):1831–40. https://doi.org/10.1109/TPWRS.2012.2194313.
[29] Shayeghi H, Shayanfar H, Jalilzadeh S, Safari A. Design of output feedback UPFC controller for damping of electromechanical oscillations using PSO. Energy Convers Manage 2009;50(10):2554–61. https://doi.org/10.1016/j.enconman.2009.06.005. URL:http://www.sciencedirect.com/science/article/pii/S0196890409002234.
[30] Salim RH, Oleskovicz M, Ramos RA. Power quality of distributed generation systems as affected by electromechanical oscillations – definitions and possible solutions. IET Gener Transm Distrib 2011;5(11):1114–23. https://doi.org/10.1049/iet-gtd.2011.0277.
[31] Tariq M, Adnan M. A load flow balancing and transient stability analysis in super smart girds using V2G. In: 2018 IEEE Power Energy Society Innovative Smart Grid Technologies Conference (ISGT); 2017 (accepted manuscript).
[32] Edomah N. Effects of voltage sags, swell and other disturbances on electrical equipment and their economic implications. In: CIRED 2009–20th International Conference and Exhibition on Electricity Distribution – Part 1; 2009. pp. 1–4. https://doi.org/10.1049/cp.2009.0502.
[33] Bendre A, Divan D, Kranz W, Brumsickle W. Equipment failures caused by power quality disturbances. In: Conference Record of the 2004 IEEE Industry Applications Conference; 2004. 39th IAS Annual Meeting, vol. 1; 2004. p. 489.https://doi.org/10.1109/IAS.2004.1348450.
[34] Lannoye E, Flynn D, O'Malley M. Transmission, variable generation, and power system flexibility. IEEE Trans Power Syst 2015;30(1):57–66. https://doi.org/10.1109/TPWRS.2014.2321793.
[35] Refaat SS, Abu-Rub H, Sanfilippo AP, Mohamed A. Impact of grid-tied large-scale photovoltaic system on dynamic voltage stability of electric power grids. IET Renew Power Gener 2018;12(2):157–64. https://doi.org/10.1049/iet-rpg.2017.0219.
[36] Georgilakis PS. Technical challenges associated with the integration of wind power into power systems. Renew Sustain Energy Rev 2008;12(3):852–63. https://doi.org/10.1016/j.rser.2006.10.007. URL:http://www.sciencedirect.com/science/article/pii/S1364032106001250.